iScience

CellPress

Article

A Read/Write Mechanism Connects p300 Bromodomain Function to H2A.Z Acetylation

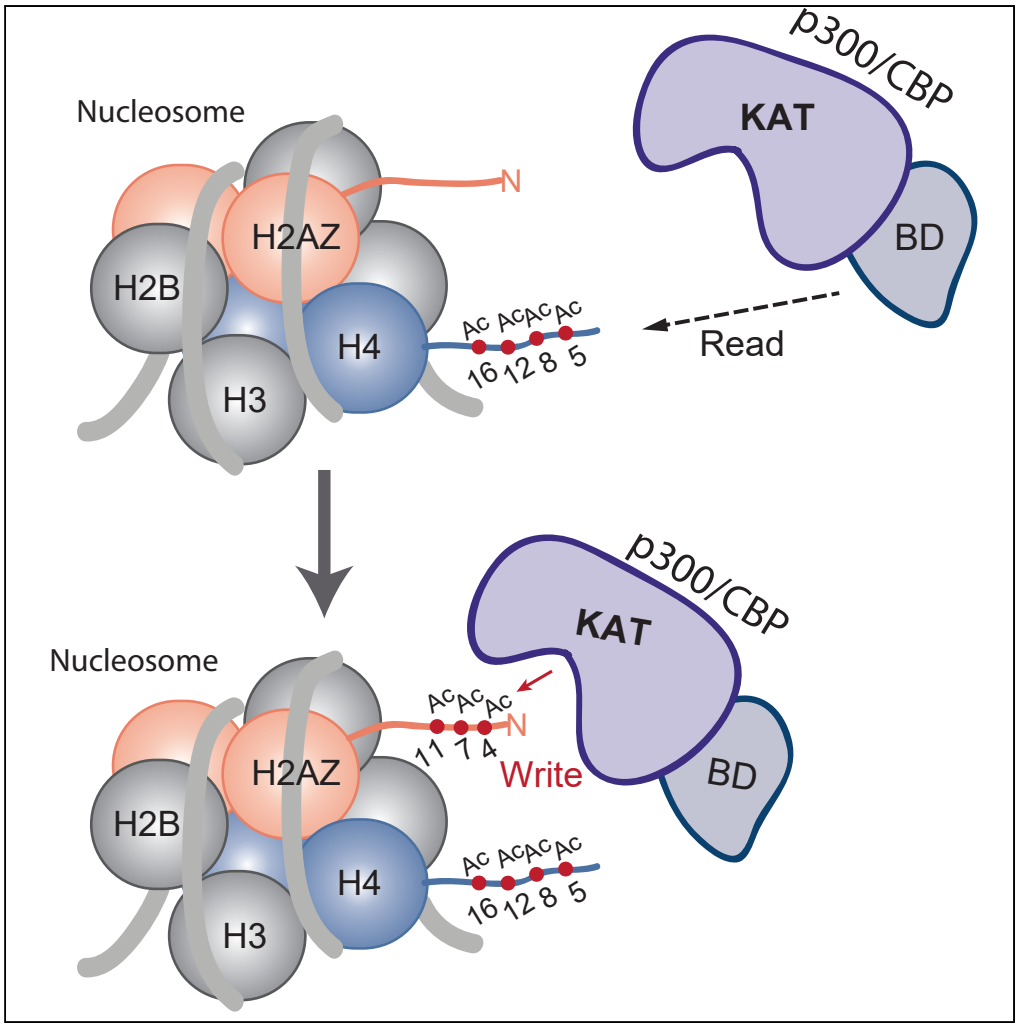

Yolanda Colino-Sanguino, Evan M. Cornett, David Moulder, ..., Scott B. Rothbart, Susan J. Clark, Fátima Valdés-Mora

scott.rothbart@vai.org (S.B.R.)
s.clark@garvan.org.au (S.J.C.)
f.valdesmora@garvan.org.au (F.V.-M.)

HIGHLIGHTS

p300 acetylates H2A.Z at multiple N-terminal lysine residues

Interaction of p300 bromodomain with H4ac enhances H2A.Zac

H2A.Zac and H4ac co-localize at active regulatory regions

H4ac and H2A.Zac differential signature can define the enhancer state

Colino-Sanguino et al., iScience *21*, 773–788
November 22, 2019
https://doi.org/10.1016/j.isci.2019.10.053

iScience

CellPress

Article

A Read/Write Mechanism Connects p300 Bromodomain Function to H2A.Z Acetylation

Yolanda Colino-Sanguino,[1,2,3,7] Evan M. Cornett,[4,7] David Moulder,[1,2,3] Grady C. Smith,[2,3] Joel Hrit,[5] Eric Cordeiro-Spinetti,[5] Robert M. Vaughan,[5] Krzysztof Krajewski,[6] Scott B. Rothbart,[5,8,*] Susan J. Clark,[2,3,8,*] and Fátima Valdés-Mora[1,2,3,8,9,*]

SUMMARY

Acetylation of the histone variant H2A.Z (H2A.Zac) occurs at active regulatory regions associated with gene expression. Although the Tip60 complex is proposed to acetylate H2A.Z, functional studies suggest additional enzymes are involved. Here, we show that p300 acetylates H2A.Z at multiple lysines. In contrast, we found that although Tip60 does not efficiently acetylate H2A.Z *in vitro*, genetic inhibition of Tip60 reduces H2A.Zac in cells. Importantly, we found that interaction between the p300-bromodomain and H4 acetylation (H4ac) enhances p300-driven H2A.Zac. Indeed, H2A.Zac and H4ac show high genomic overlap, especially at active promoters. We also reveal unique chromatin features and transcriptional states at enhancers correlating with co-occurrence or exclusivity of H4ac and H2A.Zac. We propose that differential H4 and H2A.Z acetylation signatures can also define the enhancer state. In conclusion, we show both Tip60 and p300 contribute to H2A.Zac and reveal molecular mechanisms of writer/reader crosstalk between H2A.Z and H4 acetylation through p300.

INTRODUCTION

Histone variants replace core histones to perform a variety of specialized functions (Kamakaka and Biggins, 2005) and, as canonical histones, are prone to posttranslational modifications (PTMs). H2A.Z is an evolutionarily conserved histone variant of the canonical histone H2A, which shares ~60% identity in amino acid sequence (reviewed in Zlatanova and Thakar, 2008). H2A.Z has been implicated in many diverse and potentially opposing functions, including regulation of gene transcription, where H2A.Z has been associated with active, poised, or inactive gene expression. The contrasting roles of H2A.Z are associated with different PTMs, including lysine acetylation, monoubiquitination, and methylation (reviewed in Sevilla and Binda, 2014) (Colino-Sanguino et al., 2016).

Acetylated H2A.Z (H2A.Zac) is associated with active transcription (Bruce et al., 2005; Halley et al., 2010; Millar et al., 2006; Valdes-Mora et al., 2012) and promotes nucleosome destabilization and an open chromatin conformation (Ishibashi et al., 2009). In mammals, lysines 4, 7, and 11 (K4, K7, K11) in the H2A.Z N-terminal tail are the most frequently acetylated residues (Ishibashi et al., 2009). Genome-wide studies based on H2A.Zac ChIP on-chip or ChIP-seq in different cell types and organisms have revealed that the acetylated H2A.Z forms are primarily restricted to genomic regulatory regions, such as promoters and enhancers (Bruce et al., 2005; Brunelle et al., 2015; Hu et al., 2013; Ku et al., 2012; Millar et al., 2006; Valdes-Mora et al., 2017; Valdes-Mora et al., 2012). We and others have shown that H2A.Zac is associated with aberrant gene expression in prostate (Dryhurst et al., 2012; Valdes-Mora et al., 2012) and breast cancer (Bellucci et al., 2013; Dalvai et al., 2012, 2013). Recently, we found that increased H2A.Zac levels correlate with poor prognosis in prostate cancer patients and demonstrated a pro-oncogenic role for H2A.Zac through the ectopic activation of cancer-related enhancers (Valdes-Mora et al., 2017). Collectively, these data suggest that inhibition of H2A.Z acetylation may be a therapeutic strategy for treating prostate cancer. However, the molecular mechanisms and key players responsible for the acetylation of H2A.Z are not fully understood.

Histone lysine acetylation is catalyzed by lysine acetyltransferases (KATs). In mammalian cells, nine nuclear KATs have been identified, from which three—Tip60, CREB binding protein (CBP), and E1A binding protein p300 (p300) —can acetylate canonical histones (Ito et al., 2000; Jeong et al., 2011). In the budding yeast *Saccharomyces cerevisiae*, the lysine acetyltransferase NuA4, considered the orthologue of Tip60 (Doyon et al., 2004), is reported to acetylate Htz1, the yeast orthologue of H2A.Z (Altaf et al., 2010; Keogh et al., 2006; Millar et al., 2006). Indeed, studies in mammalian cells have suggested a link between H2A.Zac

[1]Histone Variants Group, Genomics and Epigenetics Division, Garvan Institute of Medical Research, Sydney, NSW, Australia

[2]Epigenetics Research Laboratory, Genomics and Epigenetics Division, Garvan Institute of Medical Research, Sydney, NSW, Australia

[3]St. Vincent's Clinical School, University of NSW Sydney, Sydney, NSW, Australia

[4]Department of Biochemistry and Molecular Biology, Indiana University School of Medicine, Indianapolis, IN, USA

[5]Center for Epigenetics, Van Andel Institute, Grand Rapids, MI, USA

[6]Department of Biochemistry and Biophysics, University of North Carolina at Chapel Hill, Chapel Hill, NC, USA

[7]These authors contributed equally

[8]Senior author

[9]Lead Contact

*Correspondence: scott.rothbart@vai.org (S.B.R.), s.clark@garvan.org.au (S.J.C.), f.valdesmora@garvan.org.au (F.V.-M.)

https://doi.org/10.1016/j.isci.2019.10.053

and the Tip60 complex in locus-specific experiments (Dalvai et al., 2012, 2013; Giaimo et al., 2018) and by immunoprecipitation of the Tip60 complex followed by KAT assays with recombinant H2A.Z (Ito et al., 2018). However, other studies showed that H2A.Zac was independent of Tip60 inhibition at locus-specific sites (Bellucci et al., 2013; Narkaj et al., 2018) and in the context of DNA repair (Semer et al., 2019), suggesting that other KATs may also be responsible for H2A.Zac.

CBP and p300 (also known as CREBBP or KAT3A and EP300 or KAT3B, respectively) are highly homologous proteins that comprise a unique KAT family and are often referred to interchangeably. p300/CBP is a transcriptional co-activator and catalyses lysine 27 acetylation of histone H3 (H3K27ac) at promoters and enhancers (Creyghton et al., 2010; Hilton et al., 2015). p300/CBP is a multifunctional protein that acts as both a "writer" and a "reader" of lysine acetylation through its KAT domain and bromodomain (BD), respectively (Dancy and Cole, 2015; Zeng et al., 2008). p300/CBP is a promiscuous KAT that can acetylate all four canonical histones (Weinert et al., 2018). However, p300/CBP's ability to acetylate and/or interact with H2A.Z has not been critically evaluated.

In this study, we have interrogated two of the most likely KAT candidates for the acetylation of H2A.Zac: Tip60 and p300/CBP. Here, we provide *in vitro* evidence, with peptide and recombinant nucleosome substrates, that Tip60 does not efficiently acetylate H2A.Z. In contrast, we demonstrate that p300 can acetylate H2A.Z at multiple lysine residues, both *in vitro* and in human cells, and H2A.Zac is enhanced by p300 BD-mediated H4ac reader activity. In support of this mechanism, we find a high degree of genomic overlap between H2A.Zac and H4ac at active regulatory regions, preferentially at active promoters. However, at enhancers, we find that H2A.Zac and H4ac nucleosome occupancy is differentially associated with distinct chromatin features and the transcriptional activity of the genomic region. Overall, our findings suggest that in addition to Tip60, p300/CBP is also required for H2A.Z acetylation, providing new insights for the modulation of H2A.Zac pro-oncogenic activity in prostate cancer.

RESULTS

p300 Acetylates H2A.Z *In Vitro*

To test whether our putative KAT candidates acetylated H2A.Z, we performed *in vitro* lysine acetyltransferase assays with recombinant Tip60 and p300 (Figures S1A and S1B). As substrates, we used biotinylated peptides corresponding to the first 19 amino acids of H2A.Z (Figure 1A) and observed acetylation rates by measuring radioactive acetyl group incorporation (Figure 1B). As a negative control, we used an H2A.Z peptide containing the most commonly acetylated lysines (K4, K7, and K11) (Hu et al., 2013; Ishibashi et al., 2009). For positive controls, known substrates for each KAT were used, including an H4 N-terminal peptide for Tip60 (Kimura and Horikoshi, 1998) and an H3 peptide flanking H3K27 for p300 (Jin et al., 2011). Recombinant Tip60 rapidly acetylated the positive control H4 peptide. However, H2A.Z only showed a slight increase in acetylation signal compared with the negative control H2A.ZK4acK7acK11ac (Figure 1B, upper panel and Figure S1C). These data suggest that H2A.Z peptides are not optimal substrates for recombinant Tip60. In contrast, recombinant p300 (catalytic domain plus BD) (Figure S1A), which shares 82% of protein domain identity with CBP, acetylated H2A.Z peptides at a similar rate to its most appreciated histone substrate, H3K27 (Figure 1B, bottom panel). We confirmed this activity with full-length recombinant p300 (Figure S1D). p300 activity toward peptide substrates of H2A.Z isoform 2 (Dryhurst et al., 2009) was similar to isoform 1 (referred herein as H2A.Z) (Figures S1E and S1F).

H2A.Z-containing nucleosomes have slightly different biophysical properties than those containing canonical H2A, including an extended acidic path on the nucleosome surface (Suto et al., 2000), which may affect the interactions with KAT domains. To confirm our peptide results on more physiologically relevant substrates, we performed *in vitro* KAT assays using recombinant mononucleosome substrates (Figures 1C and 1D). Reactions were separated by gel electrophoresis and incorporation of tritiated acetyl groups was detected using autoradiography, allowing deconvolution of which histones were acetylated. Consistent with our peptide results, recombinant Tip60 acetylated H4 in both canonical and H2A.Z-1-containing nucleosomes (Figure 1C); however, no acetylation of H2A.Z was detected. Moreover, we found Tip60 autoacetylation, which positively regulates Tip60 catalytic activity (Yang et al., 2012), suggesting that the recombinant Tip60 is functionally active. In contrast, p300 acetylated all histones in the canonical nucleosomes after 30 min of incubation (Figure 1D), as previously reported (Ogryzko et al., 1996; Schiltz et al., 1999). Notably, p300 also acetylated all histones in the H2A.Z-1- and H2A.Z-2-containing nucleosomes, including both H2A.Z isoforms (Figure 1D). Canonical nucleosomes were a slightly better substrate than

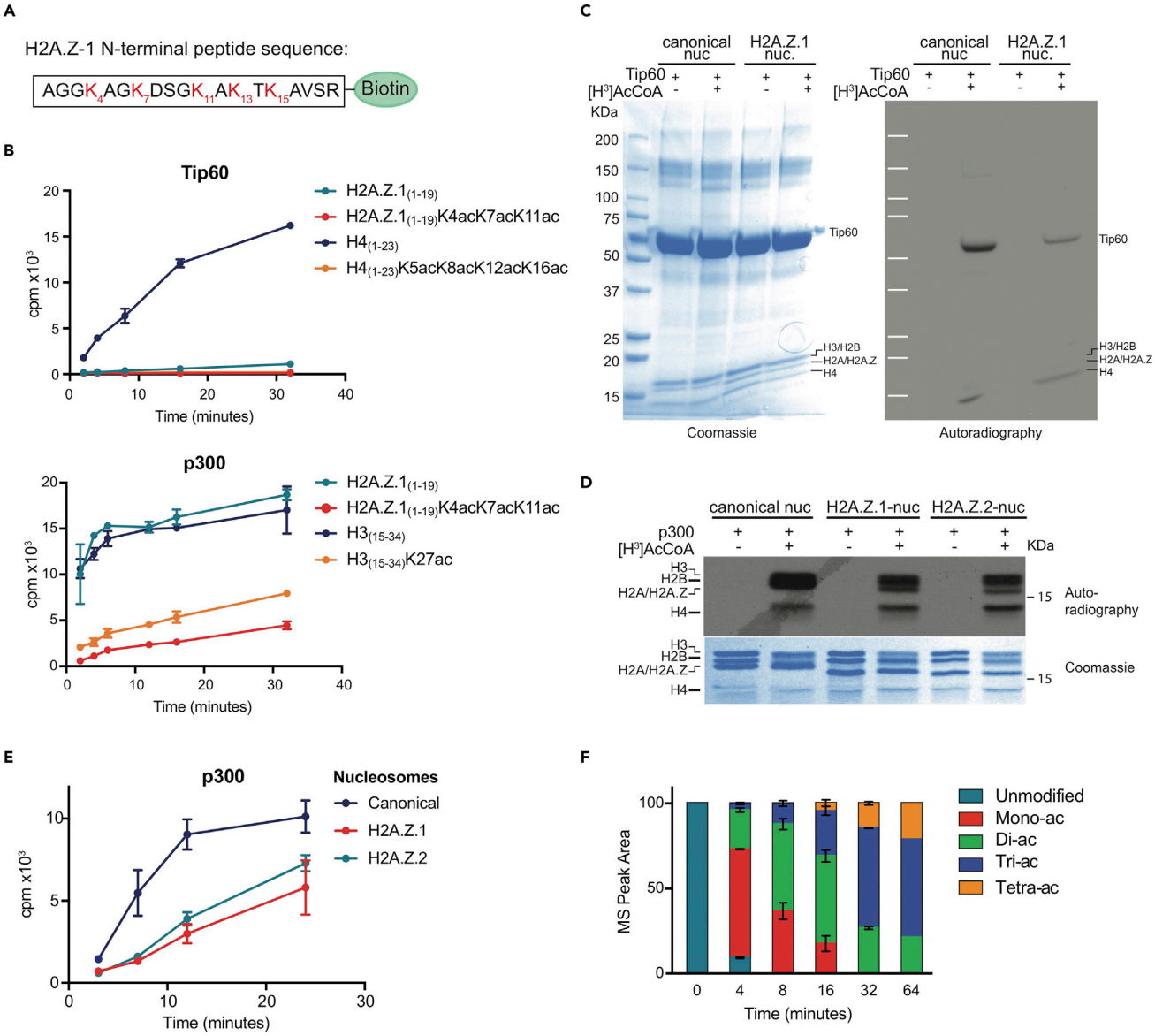

Figure 1. H2A.Z Is a Substrate for p300 *In Vitro* Assays

(A) H2A.Z-1 N-terminal amino acid sequence for the peptides used in panel (B). All lysines that can be acetylated are shown in red.

(B) In-solution H^3-Acetyl-CoA (AcCoA) assays measuring Tip60 (top) and p300 (bottom) activity as a function of time on the following histone peptide substrates: un-acetylated H2A.Z (peptide spans from amino acid 1–19, H2A.Z-1 $_{(1-19)}$) and the tri-acetylated H2AZ at lysines 4, 7, and 11 (1–19) (H2A.Z-1 $_{(1-19)}$K4acK7acK11ac) were used for both Tip60 and p300 assays. As controls we used H4 (1–23) and acetylated H4 at lysines 5, 8, 12, and 16 (1–23) ($H4_{(1-23)}$K5acK8acK12acK16ac) for Tip60 and H3 (15–34) and acetylated H3 at lysine 27 peptides (15–34) ($H3_{(15-34)}$K27ac) for p300. Data points are presented as mean count per minute (cpm). Error bars represent the standard deviation (SD) from two measurements.

(C) Coomassie staining (left) and H^3 fluorography (right) of recombinant canonical nucleosomes (canonical nuc) and homotypic H2A.Z-1 nucleosomes (H2A.Z-1 nuc) incubated with Tip60 in the presence or absence of H^3-AcCoA for 12 h. White bands in the autoradiography are the overlayed molecular weight markers shown in the Coomassie staining. Representative image of two replicates.

(D) H^3 fluorography (top) and Coomassie staining (bottom) of recombinant canonical nucleosomes (canonical nuc) and homotypic H2A.Z-1 and H2A.Z-2 nucleosomes (H2A.Z-1/H2A.Z-2 nuc) incubated with p300 in the presence or absence of H^3-AcCoA for 30 min. Representative image of two replicates.

(E) In-solution H^3-AcCoA KAT assays measuring p300 activity as a function of time on nucleosome substrates, as indicated. Data points are presented as mean count per minute (cpm). Error bars represent the SD from two measurements.

(F) Percentage of area under the mass spectrometry (MS) peak of unacetylated, one acetylated lysine (mono-ac), two acetylated lysines (di-ac), three acetylated lysines (tri-ac), or four acetylated lysines (tetra-ac) from H2A.Z peptides at increasing p300 incubation time points, 0, 4, 8, 16, 32, and 64 min (raw data are displayed in Figure S2.). Data are represented as mean −/+ SD of two independent replicates.

See also Figures S1 and S2.

variant-containing nucleosomes, but no differences were found in the acetylation rates between nucleosomes containing H2A.Z-1 and H2A.Z-2 isoforms (Figure 1E).

Mass spectrometry data from human cells have shown that H2A.Zac is found most commonly as a tri-acetylated form, with lysines 4, 7, and 11 (K4, K7 and K11) carrying acetyl groups (Hu et al., 2013; Ishibashi et al., 2009). To determine whether p300 acetylates these residues, we used mass spectrometry to map acetylation sites on H2A.Z N-terminal peptide after reaction with p300 (Figures 1F and S2A). By four minutes, 90% of all peptides were acetylated, and unacetylated peptides were not detectable in the subsequent time points. Mono-acetylated (mono-ac) peptides were only present after 4, 8, or 16 min, and the proportion decreased by half over the time course (63.6%, 36.9%, and 17.8%, respectively). In contrast, tetra-acetylated peptides were detected (14.4% and 21.1%) at the longest time points (32 and 64 min). Tandem MS analysis showed that all lysines on the N-terminus of H2A.Z (K4, K7, K11, K13, and K15) could be acetylated by p300, but K4 and K7 were preferred (Figure S2B).

In summary, we provide biochemical evidence that the lysine acetyltransferase Tip60 alone is not sufficient to acetylate H2A.Z. In contrast, we show that p300 on its own rapidly acetylates both H2A.Z peptides and H2A.Z-containing nucleosomes at multiple N-terminal lysines.

Inhibition of p300 and Tip60 Decreases H2A.Zac

To determine whether p300 and Tip60 acetylate H2A.Z in cells, we used A-485, a recently developed and highly selective and potent inhibitor for p300/CBP KAT domains (Lasko et al., 2017) (Figure 2A), as well as genetic inhibition of Tip60, p300, and CBP by siRNA in two human cancer cell lines (LNCaP and HCT116) (Figures 2B and 2C). We isolated chromatin fractions from all conditions and performed Western blot analysis. To test changes in H2A.Z acetylation, we used three antibodies against different H2A.Z acetylation forms: H2A.Ztri-ac (K4, K7 and K11), H2A.ZK4ac, and H2A.ZK7ac. We characterized the antibody substrate affinity by peptide microarray, as previously described (Rothbart et al., 2012a). We found that H2A.Ztri-ac specifically recognizes the tri-acetylated form of H2A.Z; H2A.ZK4ac binds to substrates that contain H2A.Z-K4ac but does not distinguish between degrees of acetylation, whereas H2A.ZK7ac binds exclusively to mono-acetylated H2A.Z at K7 (Figure S3).

Using these antibodies, we found that cells treated with A-485 had a strong and consistent dose-dependent reduction of the positive control H3K27ac between cell lines, whereas the less specific substrate, H4tetraAc, did not show a clear reduction (Figure 2A). Signal from the H2A.Ztri-ac antibody did not show a significant reduction in either of the cell lines, whereas H2A.ZK4ac and H2A.ZK7ac showed a clear dose-dependent decrease. At 10 μM concentration of A-485, the mono-acetylated H2A.Z antibodies showed an average reduction of 67% and 92% in LNCaP and HCT116 cells, respectively. No clear differences were detected between the reduction of H2A.ZK4ac and H2A.ZK7ac. These data suggest that inhibition of p300/CBP by A-485 preferentially reduces H2A.ZK4ac and H2A.ZK7ac mono-acetylated forms.

There are currently no selective Tip60 inhibitors commercially available. Therefore, we performed siRNA knockdown (KD) experiments to investigate the effects on H2A.Zac (Figures 2B and 2C). Tip60 mRNA levels were reduced by 87% and protein abundance by 80% following Tip60 KD (Figures 2B and 2C). H2A.Zac was significantly reduced after Tip60 KD, 58% for the triAc, 45% for K4ac, and 79% for K7ac (Figure 2C), as previously reported in Tip60 conditional knockout experiments (Li et al., 2019). We found that the tetra-acetylated form of H4 was reduced by 64%, in line with our cell-free assays. We also performed siRNA experiments for the double p300/CBP KD and a triple p300/CBP/Tip60 KD. Even though the mRNA levels of p300 and CBP in the double KD were moderately decreased (~50% and 32%, respectively, Figure 2B), the positive control H3K27ac was reduced by 92% (Figure 2C), suggesting the HAT inhibition was enough to detect changes in the histone acetylation profile. Interestingly, Tip60 mRNA levels increased by two-fold after p300/CBP KD but this did not translate to a significant change of Tip60 protein level (Figure 2B). The double p300/CBP KD reduced all H2A.Zac forms to a similar ratio as the Tip60 KD (Figure 2C). However, the triple KD of CBP, p300 and Tip60 showed a greater reduction of H2A.Z acetylation in comparison to the single Tip60 or p300/CBP KDs (Figures 2B and 2C). Interestingly, K7 acetylation was the most reduced in all KD combinations, with 97% reduction in the triple KD.

A recent resource paper mapped the p300 acetylome in mammals using quantitative mass spectrometry after genetic or chemical modulation of p300 activity (Weinert et al., 2018). We analyzed this H2A.Z

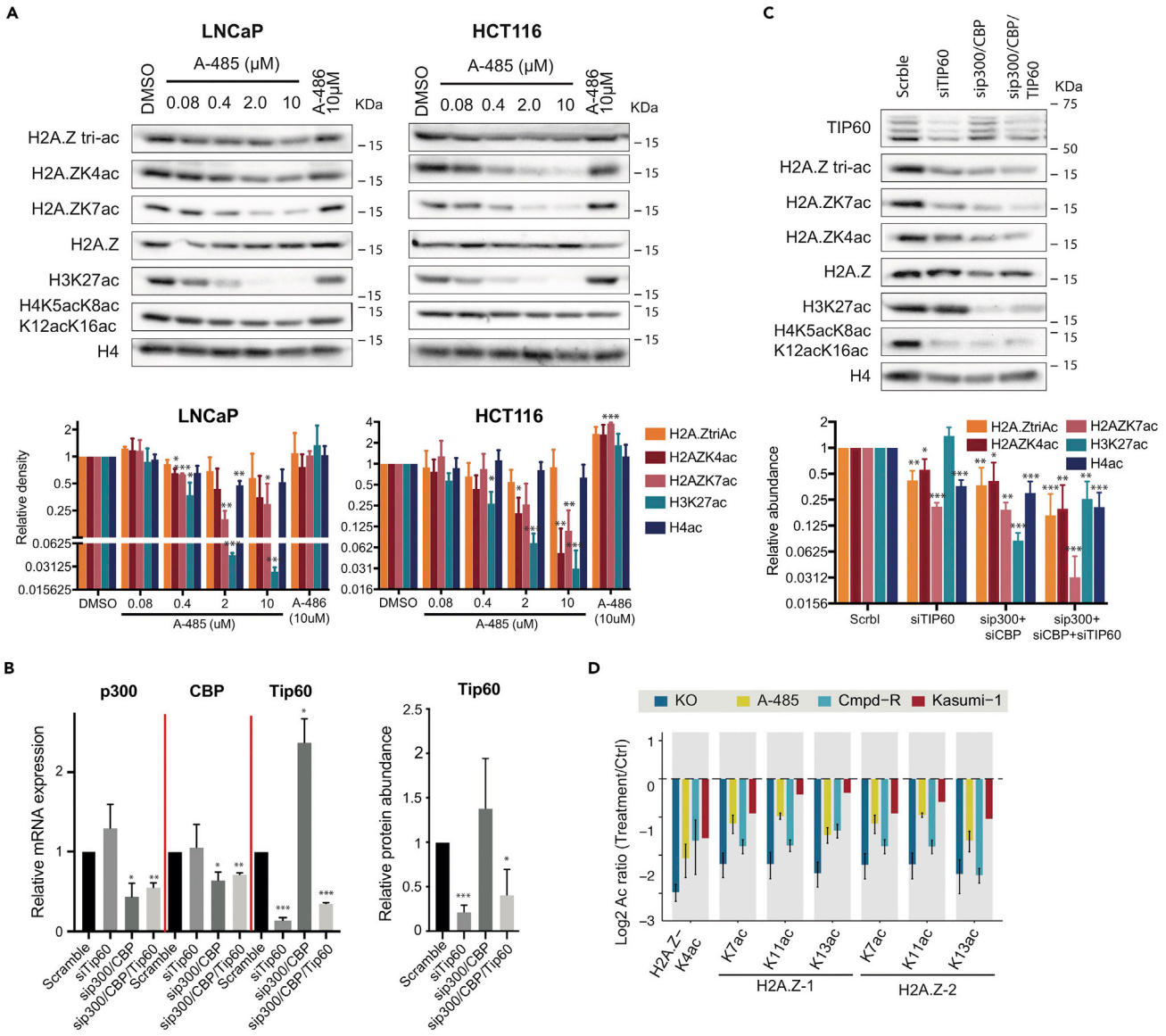

Figure 2. Inhibition of Tip60 and p300 Decrease H2A.Z Acetylation in Cancer Cell Lines

(A) Western blot analysis of chromatin purified extracts from LNCaP and HCT116 cells treated with A-485 for 24 h at increasing concentrations (0.08, 0.4, 2, and 10 μM). The compound A-486, an inactive analog of A-485, was also used as negative control. The figure shows a representative image of two biological replicates (top) and densitometry quantification (bottom). Densitometry quantification of histone acetylation abundance is shown at the bottom, and it is represented as the relative amount to DMSO control in logarithmic scale. H2A.Z acetylation forms were normalized to total H2A.Z; H3K27ac and H4ac were normalized to H4. Data are represented as mean and SD (n = 2). Student's t-test was performed to compare each condition to DMSO. *p value<0.05, **p value<0.01, ***p value<0.001.

(B) Quantification of the knockdown (KD) levels of the siRNA experiments by mRNA expression (left panel) and protein abundance of TIP60 (right panel). Cells were transfected with a pool of four siRNAs for Tip60 and CBP and three siRNAs for p300 (See Table S3 for siRNA sequences). The pools were then combined accordingly for the double p300/CBP KD and triple p300/CBP/Tip60 KD. mRNA expression of Tip60, p300, and CBP was measured by real-time qPCR in cells transfected with Tip60, p300, and CBP siRNAs (left). mRNA levels of all conditions were calculated relative to untargeted siRNA control (scramble). Data are represented as mean and SD (n = 2), and Student's t-test was performed to compare each condition to scramble. Densitometry quantification of each Tip60 band was normalized to the loading control H4 and relative to scramble, and it is represented as logarithmic scale. The mean relative abundance of each band and SD was plotted and Student's t-test was performed to compare each condition to scramble. *p value<0.05, **p value<0.01, ***p value<0.001. Find list of siRNA and primer sequences in Tables S3 and S4, respectively.

(C) Western blot analysis of the chromatin fractions from LNCaP cells transfected with the scramble control (Scrble) Tip60 siRNA (siTIP60), p300, and CBP siRNAs (sip300/CBP) or p300, CBP, and Tip60 siRNAs (sip300/CBP/TIP60). The figure shows a representative image of at least two biological replicates (top) and densitometry quantification (bottom). Histone acetylation abundance was measured by densitometry and calculated relative to the scramble control.

Figure 2. *Continued*

Data are represented as mean and SD (n = 2 or more). The graph is shown in a logarithmic scale, and Student's t-test was performed to compare each condition to scramble. *p value<0.05, **p value<0.01, ***p value<0.001.

(D) Weinert et al.'s acetylome mass spectrometry data after CBP/p300 perturbations, including double knockout of p300 and CBP genes (KO, dark blue) and chemical inhibition with A-485 (A-485, yellow) and compound-R (Cmpd-R, light blue) in mouse embryonic fibroblasts cells. Kasumi-1 cells, a human acute myeloid leukemia cell line, were treated with compound-R (red). *Log2* SILAC normalized ratios for each detectable acetylation site of H2A.Z-1 and H2A.Z-2 isoforms were plotted. SILAC normalized ratios were calculated as explained in Weinert et al. (2018). The peptides containing K4ac are identical between isoforms, and therefore, they were analyzed as one. Error bars represent standard error of three independent replicates when available.

See also Figure S3 and Tables S1, S3, and S4.

acetylation data and confirmed our *in vitro* and in-cell results (Figure 2D). Consistently, H2A.Z acetylation at lysines K4, K7, K11, and K13 was reduced after chemical inhibition of p300 KAT activity in both MEFs and Kasumi-1 cell lines (Figure 2D). The greatest effect was observed in the p300/CBP double knockout. Taken together, these data strongly support the conclusion that p300/CBP is a major KAT for H2A.Z in cells. We found that although Tip60 can modulate acetylation levels of H2A.Zac, it is not the sole KAT for H2A.Z and that p300/CBP is also essential for the acetylation of H2A.Z (Figure 6A).

Interaction of p300 BD with H4ac Promotes p300-mediated H2A.Z Acetylation *In Vitro*

Previous studies have shown that p300 BD binds H4ac, thereby acting as a reader of histone acetylation (Delvecchio et al., 2013; Nguyen et al., 2014). Interestingly, there is high sequence homology between H4 and H2A.Z at their N-termini (Figure S4A), where the spacing of the lysines follow the same $KAc(X)_{2–3}KAc$ pattern, in which X represents any amino acid, which is reported to have the strongest p300 BD binding (Delvecchio et al., 2013). We questioned whether the p300 BD was also capable of reading H2A.Zac. Using histone peptide arrays printed with approximately 260 uniquely modified histone peptides (Cornett et al., 2016), including major single and combinatorial acetylations on all four core histones and the variant H2A.Z (see Table S1), we revealed that p300 BD binds exclusively to H4-acetylated peptides (Figures 3A and S4B). No binding was measured for acetylated H2A.Z or any other acetylated histone peptide in the library.

A feedforward mechanism of p300-dependent H3K27 acetylation through BD recruitment to H4ac has been previously proposed (Nguyen et al., 2014). Indeed, in our *in vitro* KAT assays, the rate of p300 acetylation on nucleosomes pre-installed with H4ac was faster than unmodified nucleosomes (Figure 3B). Thus, we hypothesized that the p300 BD interaction with H4ac may also enhance H2A.Z acetylation. To test this hypothesis, we first performed a time course radioactive KAT assay with recombinant p300 and H2A.Z-containing nucleosome substrates (Figure 3C). As expected, we observed time-dependent acetylation on all nucleosomal histones. Notably, H2A.Z acetylation trailed H4 acetylation in this time course.

We next used the p300 BD inhibitor, CBP30 (Conery et al., 2016; Hammitzsch et al., 2015), to further question whether p300 BD activity impacts H2A.Z acetylation. Using the same peptide array approach, we validated that CBP30 completely blocks the p300 BD from binding to H4-acetylated peptides (Figures 3D, S4C, and S4D). We performed *in vitro* KAT assays in the presence and absence of CBP30 using recombinant canonical, H2A.Z-containing, and H4ac-containing nucleosomes. Inhibition of the p300 BD resulted in decreased acetylation of all histones, including histone H2A.Z (Figure 3E). To further validate that BD recruitment enhances p300-mediated H2A.Z acetylation, we treated HCT116 cells with CBP30 for 24 h using a concentration range (1–10uM), recommended by Conery et al., 2016 (Figure 3F). We observed a reduction in H3K27ac levels, as previously reported (Raisner et al., 2018). Notably, there was also a decrease in H2A.Zac levels, where H2A.ZK7ac showed a striking reduction of up to 90%. Taken together, these data suggest that acetylation of H2A.Z by p300 is enhanced upon recruitment to H4-acetylated nucleosomes via the p300 BD.

H2A.Zac and H4K5ac Co-occur at Promoter Regions

We next sought to determine whether H2A.Zac- and H4ac-marked nucleosomes co-exist in the chromatin. To address this, we determined the genomic distribution of both marks using publicly available ChIP-seq data for H2A.Zac and H4K5ac in LNCaP cells (Table S2). The specificity of both antibodies was characterized with histone peptide arrays (Rothbart et al., 2012a; Dickson et al., 2016) (Figure S3A for H2A.Ztri-ac and http://www.histoneantibodies.com/ for H4K5ac). As previously reported (Rothbart et al., 2012b, 2015), the H4K5ac antibody bound preferentially to H4 peptides that also have acetylation at other sites forming

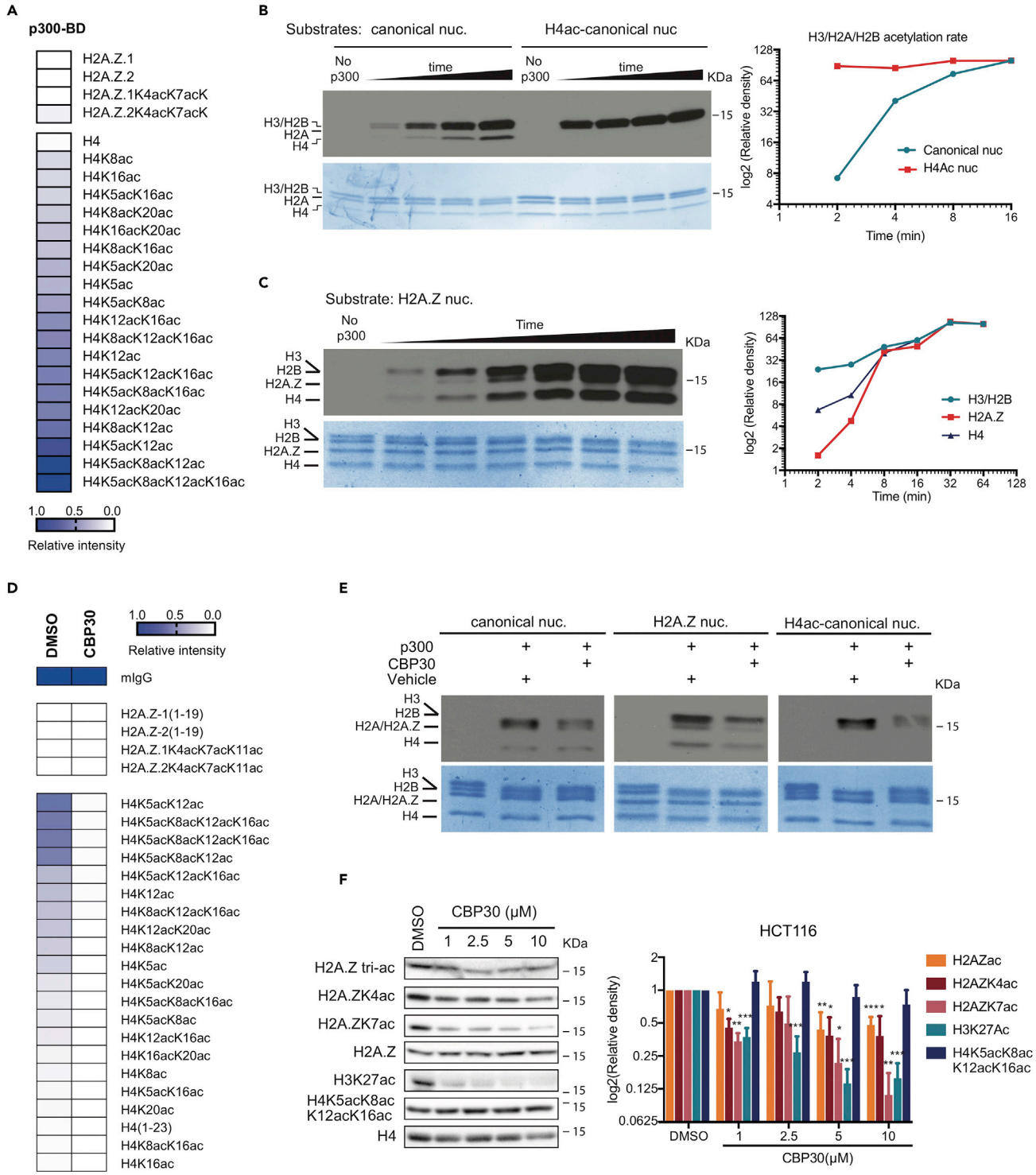

Figure 3. Bromodomain Binding to H4-Acetylated Tail Enhances H2A.Z Acetylation

(A) Heatmap showing p300 BD binding preference for H2A.Z and H4 peptides from histone peptide microarray analysis. Scalebar shows the color key to the relative intensity, normalized to the peptide with the highest raw signal (H4K5acK8acK12acK16ac). Data are represented as mean normalized signal (n = 6). Array 1 was used for this experiment. The complete list of peptides included in the histone peptide microarray is in Table S1.

(B) H^3 fluorography (top) and Coomassie staining (bottom) of H2A canonical nucleosomes (canonical nuc) or H4K5acK8acK12acK16ac pre-marked canonical nucleosomes (H4ac-canonical nuc) incubated with p300 over time (0, 2, 4, 8, and 16 min). Representative image of two experiments. The right plot shows the quantification of the acetylated band density corresponding to H2A/H2B/H3 in the canonical nucleosome and H4ac-canonical nucleosome over time.

Figure 3. *Continued*

(C) H^3 fluorography (top) and Coomassie staining (bottom) of H2A.Z-1 nucleosomes incubated with p300 over time (0, 2, 4, 8, 16, 32, and 64 min). The right plot shows the density quantificatification of H2B/H3, H2A.Z, and H4 acetylated bands over time.

(D) Heatmap showing p300 BD binding preference for H2A.Z and H4 peptides in the presence or absence of CBP30 inhibitor from histone peptide microarray analysis. DMSO was used as vehicle control. Scalebar shows the color key to the relative intensity, normalized to the IgG positive control of each array. Data are represented as mean normalized signal (n = 6). Array 1 was used for this experiment. The complete list of peptides included in the histone peptide microarray is in Table S1.

(E) H^3 fluorography (top) and Coomassie staining (bottom) of canonical, H2A.Z-1 and H4K5acK8acK12acK16ac modified canonical nucleosomes incubated with p300 in the presence of CBP30 or DMSO as indicated.

(F) Western blot analysis of HCT116 cells treated with CBP30 for 24 h at increasing concentrations (1, 2.5, 5, and 10 μM). Representative image of at least two biological replicates (top) and densitometry quantification represented in logarithmic scale (bottom). Protein abundance was calculated relative to DMSO control, and data are represented as mean and SD (n = 2). Student's t-test was performed to compare each condition to DMSO. *p value<0.05, **p value<0.01, ***p value<0.001.

See also Figure S4 and Table S1.

di-, tri-, and tetra-acetylation states. Thus, we considered H4K5ac ChIP-seq data as reporting on H4 N-terminal tail poly-acetylation (referred to herein as H4ac), a signature consistent with the binding activity of p300 BD (Figure 3A).

We first investigated the co-occurrence of H2A.Zac and H4ac ChIP-seq peaks genome-wide and found a significant overlap, with 51.8% of H2A.Zac peaks coinciding with H4ac (Figure 4A). To consider the predicted functional properties, we used ChromHMM (Ernst and Kellis, 2012) to demarcate six different genomic regulatory regions based on the information from six chromatin marks (Figure S5A and Table S2). We found that H4ac had a similar functional distribution pattern as H2A.Zac (Valdes-Mora et al., 2017), where it was significantly enriched at promoters and enhancers and depleted at polycomb and transcribed regions (Figure S5B). To address whether the epigenetic context impacts the coexistence of H2A.Zac and H4ac, we also performed ChromHMM analysis of the overlapping marked peaks (23,904 regions, called common peaks) and unique marked peaks for H2A.Zac or H4ac (20,876 and 15,460 regions, called H2A.Zac- or H4ac-unique peaks, respectively) (Figure 4B). We found that the common peaks were most significantly located at active promoters: 51.64% of the common peaks (Figure 4B, upper panel) and 68.74% of all active promoters (Figure 4C). In contrast, the uniquely marked regions were more prevalent at enhancers (Figure 4B, middle and bottom panels), where most of the H2A.Zac-unique peaks occurred at active enhancer regions (Figure 4B, middle panel), whereas H4ac-unique peaks were mostly enriched at poised enhancers (Figure 4B, bottom panel). However, at distal regulatory regions, we observed that both common and unique regions were present in different proportions (Figure 4D), suggesting a dynamic interplay of these two marks.

Epigenetic Characteristics of Enhancers with Differential Distribution of H2A.Zac and H4ac

In order to further define the patterns of H2A.Zac- and H4ac-marked nucleosomes at enhancers, we examined different epigenetic features at these regions, including H2A.Z, p300, and H3K27ac, DNA methylation, and chromatin accessibility (Table S2). ChIP-seq data was split by H2A.Zac and H4ac signatures and ordered by H2A.Zac intensity at both poised and active enhancers (Figure 4E). Notably, we found that enhancers lacking H2A.Zac were not enriched for total H2A.Z, suggesting that enhancers with an H4ac-unique signature are also void of H2A.Z. Second, in agreement with a p300 BD-mediated recruitment mechanism proposed by this study and others (Conery et al., 2016; Manning et al., 2001), p300 showed differential occupancy between groups at both active and poised enhancers; in particular, the group lacking H4ac showed less p300 occupancy. Finally, H3K27ac, a histone PTM signature characteristic of active enhancers, did not show differential distribution between the groups, although H3K27ac intensity correlated with H2A.Zac signal. These data suggest a common pattern of acetylation of H3K27ac and H2A.Zac that may be established by p300.

We next used Nucleosome Occupancy and Methylation sequencing (NOMe-seq) data to study DNA methylation and chromatin accessibility at these enhancer sites (Kelly et al., 2012). We found that H2A.Zac-unique enhancers had less DNA methylation and were more accessible than the average of all active and poised enhancers. In contrast, H4ac-unique active and poised enhancers had more methylation and were less accessible (Figure 4F). Enhancers carrying both H2A.Zac and H4ac had similar levels of DNA methylation and accessibility as the average enhancers. In summary, we found that enhancers with differential H2A.Zac and H4ac signatures are associated with distinct epigenetic features (Figure 6B).

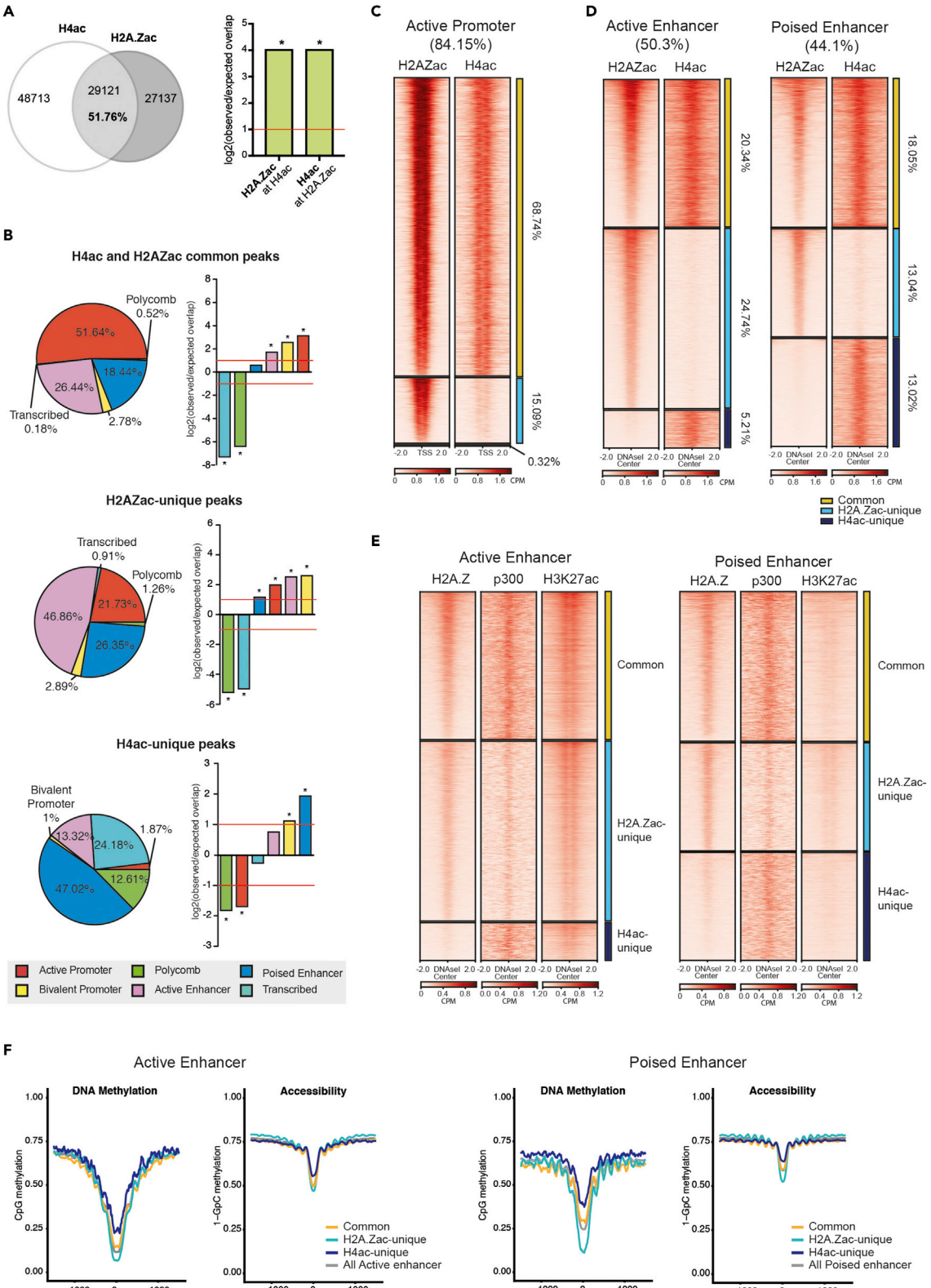
A
H4ac
H2A.Zac
48713
29121
51.76%
27137
log2(observed/expected overlap)
H2A.Zac at H4ac
H4ac at H2A.Zac
B
H4ac and H2AZac common peaks
Polycomb 0.52%
51.64%
18.44%
26.44%
Transcribed 0.18%
2.78%
log2(observed/expected overlap)
H2AZac-unique peaks
Transcribed 0.91%
Polycomb 1.26%
21.73%
46.86%
26.35%
2.89%
log2(observed/expected overlap)
H4ac-unique peaks
Bivalent Promoter 1%
13.32%
24.18%
1.87%
47.02%
12.61%
log2(observed/expected overlap)
Active Promoter
Polycomb
Poised Enhancer
Bivalent Promoter
Active Enhancer
Transcribed
C
Active Promoter (84.15%)
H2AZac
H4ac
68.74%
15.09%
0.32%
-2.0 TSS 2.0
0 0.8 1.6 CPM
D
Active Enhancer (50.3%)
Poised Enhancer (44.1%)
H2AZac
H4ac
20.34%
24.74%
5.21%
18.05%
13.04%
13.02%
-2.0 DNAseI 2.0 Center
0 0.8 1.6 CPM
Common
H2A.Zac-unique
H4ac-unique
E
Active Enhancer
Poised Enhancer
H2A.Z
p300
H3K27ac
Common
H2A.Zac-unique
H4ac-unique
-2.0 DNAseI 2.0 Center
0 0.4 0.8 CPM
F
Active Enhancer
Poised Enhancer
DNA Methylation
Accessibility
CpG methylation
1−GpC methylation
Distance from feature (bp)
Common
H2A.Zac-unique
H4ac-unique
All Active enhancer
All Poised enhancer

Figure 4. Crosstalk and Genomic Localization of H2A.Zac and H4K5ac

(A) Genomic overlap of all H2A.Zac and H4ac ChIP-seq peaks. Minimum overlap equals 1bp (left panel). Observed vs expected logarithmic fold enrichment graphs using Genomic Association Test (GAT) of H2AZ.ac over H4ac and reversely (right panel). *p value< 0.0001.

(B) GAT of H2AZ.ac and H4ac ChIP-seq peaks and ChromHMM regions in LNCaP cells. The three groups examined are H2A.Zac and H4K5ac common peaks, H2A.Zac-unique peaks, and H4K5ac-unique peaks. Pie charts representing the percentage of marked peaks falling in each ChromHMM state (left panel). Observed vs expected log-fold enrichment graphs (right panel). *p < 0.0001.

(C and D) Heatmaps showing H2A.Zac and H4ac presence across active promoters (n = 12,770) (C) and active enhancer (n = 27,898) and poised enhancers (n = 17,354) (D). Heatmaps are divided into the same three groups than panel B and order based on H2A.Zac intensity from top to bottom. ChIP-seq signal is centered at the TSS in active promoters and at the DNaseI midpoint in enhancers. The scale bars show the color key of the ChIP-seq intensity (counts per million mapped reads, CPM). The same scale is used for each ChIP-seq across all regulatory regions.

(E) Heatmaps showing H2A.Z, p300, and H3K27ac enrichment across active enhancers (left) and poised enhancers (right). Heatmaps are divided, ordered, and centered similarly to panel (D).

(F) Nucleosome occupancy and methylation sequencing (NOMe-seq) plots representing the average DNA methylation (0–1) and chromatin accessibility (1 minus GpC methylation ratio) ratios across active (left hand side) and poised enhancers (right hand side) divided into the same three groups than panel (B). The average of all active and poised enhancers is also included.

See also Figure S5 and Table S2.

Acetylation Dynamics between H2A.Z and H4 at Enhancers Is Associated with Transcription Elongation

Chromatin accessibility and DNA methylation are indicative of enhancer activity (Valdes-Mora et al., 2017). To characterize the functional status of each enhancer H4/H2A.Z acetylation signature, we examined RNA polymerase II (RNApolII) recruitment and enhancer RNA (eRNA) production (Kim et al., 2010) as additional markers of enhancer function (Table S2). Figure 5A shows RNApolII ChIP-seq signal and Global Run-on sequencing (GRO-seq) data across active and poised enhancers. eRNA production is measured as the bidirectional RNA expression detected by GRO-seq around the DNaseI midpoint. Despite no major differences between H2A.Zac/H4ac signatures in eRNA production and the presence of RNAPolII flanking DNAseI sites, we did reveal evidence of differential transcription across the entire 4kb region plotted (Figure 5A). H2A.Zac-unique enhancers had less regional transcriptional activity than the other two groups (common and H4ac-unique) in both active and poised enhancers.

To confirm that the observed transcription signal at expanded enhancers was due to transcription elongation, we grouped the enhancers according to their location inside or outside genes and compared their proportion with the rest of the enhancers (Figure 5B). A higher proportion of H4ac-unique enhancers were located at intragenic regions. H2A.Zac-unique active enhancers did not show differential localisation, whereas H2A.Zac-unique poised enhancers showed a higher presence at intergenic regions (Figure 5B). Common enhancers had similar inter/intragenic distribution to all detectable active and poised enhancers. We also found that genes with H2A.Zac-unique enhancers had significantly lower transcription compared with all genes containing either active or poised enhancers, whereas H4ac-unique enhancers were mostly present at highly expressed genes (Figure 5C). Moreover, the nascent RNA profiles measured by GROseq at intragenic enhancers validated the gene expression pattern (Figures 5D and S5C).

Taken together, these results demonstrate a particular H2A.Zac and H4ac pattern, or enhancer code, that correlates with their genomic localization (inter or intragenic), regional transcriptional activity, chromatin features (p300, chromatin accessibility), and DNA methylation (Figure 6B).

DISCUSSION

A key step to understanding histone PTM function is the characterization of the enzymes and effector proteins that write, erase, and read these marks. Although much progress has been made identifying the core histone PTM modifiers (Voss and Thomas, 2018), the specific enzymes that target histone variants PTMs have not been well studied. In particular, the KATs responsible for acetylation of H2A.Z in mammals are still unresolved. Here, we report that in addition to Tip60, p300 is able to acetylate the histone variant H2A.Z and that p300-dependent H2A.Z acetylation is enhanced through BD recognition of H4ac.

Unlike Tip60, p300 has not been described to interact with H2A.Z (Choi et al., 2009; Link et al., 2018; Obri et al., 2014; Vardabasso et al., 2015), as it potentially follows a hit-and-run kinetic mechanism (Liu et al., 2008). Tip60, however, has been described as the KAT candidate responsible for acetylation of H2A.Z (Corujo and Buschbeck, 2018; Giaimo et al., 2019; Sevilla and Binda, 2014). Tip60 is part of a larger complex, involved in H2A.Z histone exchange (Altaf et al., 2010; Cai et al., 2003; Keogh et al., 2006; Kusch

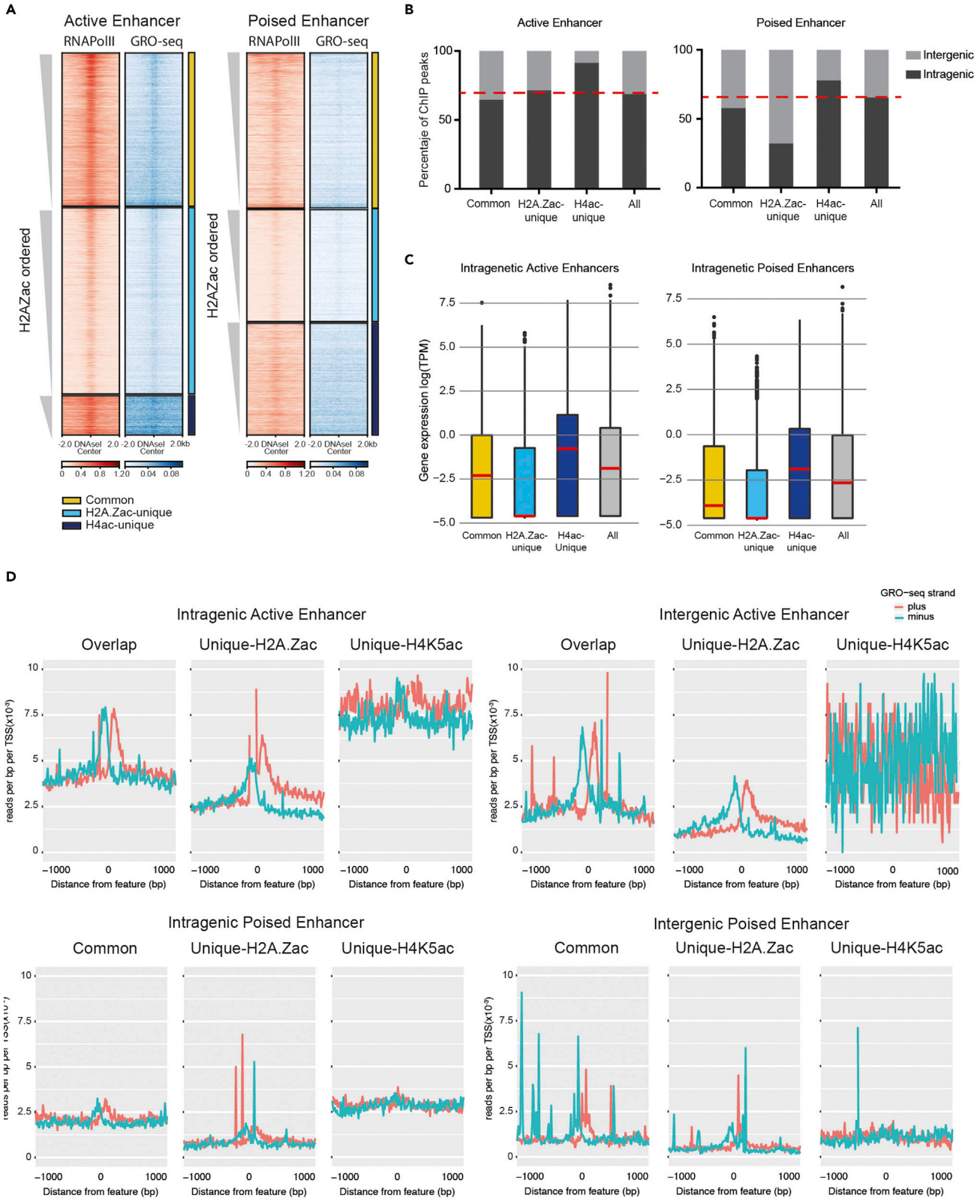
A
Active Enhancer
RNAPolII
GRO-seq
Poised Enhancer
RNAPolII
GRO-seq
H2AZac ordered
H2AZac ordered
-2.0 DNAseI Center 2.0
-2.0 DNAseI Center 2.0kb
0 0.4 0.8 1.20 0.04 0.08
Common
H2A.Zac-unique
H4ac-unique
B
Active Enhancer
Poised Enhancer
Percentaje of ChIP peaks
100
50
0
Intergenic
Intragenic
Common
H2A.Zac-unique
H4ac-unique
All
C
Intragenetic Active Enhancers
Intragenetic Poised Enhancers
Gene expression log(TPM)
7.5
5.0
2.5
0.0
−2.5
−5.0
Common
H2A.Zac-unique
H4ac-Unique
H4ac-unique
All
D
GRO−seq strand
plus
minus
Intragenic Active Enhancer
Intergenic Active Enhancer
Overlap
Unique-H2A.Zac
Unique-H4K5ac
reads per bp per TSS(x10⁻³)
10
7.5
5
2.5
0
−1000
0
1000
Distance from feature (bp)
Intragenic Poised Enhancer
Intergenic Poised Enhancer
Common
Unique-H2A.Zac
Unique-H4K5ac

Figure 5. Transcription Elongation Influences H2A.Zac and H4K5ac Landscape at Enhancers

(A) Heatmaps showing phosphoserine 5 RNA polymerase II (RNAPolII) ChIP-seq and global run-on sequencing (GRO-seq) signal across active and poised enhancers. The three groups examined are H2A.Zac and H4ac overlapping peaks (Common, yellow), H2A.Zac-unique peaks (H2A.Zac-unique, light blue), and H4ac-unique peaks (H4ac-unique, dark blue) at active (left) and poised (right) enhancers that are at least 2kb away from any TSS. Heatmaps are ordered based on H2A.Zac intensity from top to bottom. The scale bars show the color key of the ChIP-seq and GRO-seq intensities (counts per million mapped reads, CPM).

(B) Bar plots showing the proportion of intragenic (black) and intergenic (gray) active and poised enhancers in each H2A.Zac/H4ac group. The red dashed line marks the proportion of intergenic and intragenic enhancers found in all active and poised enhancers.

(C) Box plots comparing gene expression as logarithmic transcripts per million (logTPM) measured by RNA-seq of the genes contained on each intragenic active (left) or poised enhancers for each H2A.Zac/H4ac group and all the genes containing at least one enhancer (gray box plot).

(D) Bidirectional enhancer RNAs (eRNAs) profile plots (plus, red, and negative, blue-strands) of GROseq data around intragenic and intergenic active enhancers (top) and poised enhancers (bottom) of the H2A.Zac/H4ac groups. The plots show one representative replicate out of four. Profiles are centered at the DNAse I midpoint.

See also Figure S5.

et al., 2004), which makes it difficult to assess whether Tip60 alone is able to acetylate H2A.Z. In fact, our *in vitro* results show that Tip60 acetylates peptide and nucleosomal H4 but does not efficiently acetylate H2A.Z. However, we and others (Dalvai et al., 2012; Li et al., 2019) found that genetic inhibition of Tip60 decreases H2A.Zac levels, suggesting that Tip60, in its cellular context, facilitates H2A.Z acetylation. Of note, complete knockout of Tip60 does not abolish H2A.Zac (Li et al., 2019), and other reports found that acetylation of H2A.Z was independent of Tip60 at some locus-specific promoter (Bellucci et al., 2013; Semer et al., 2019), supporting our finding that p300/CBP is also required for the acetylation of H2A.Z. Based on our new data, we propose a model whereby acetylation of H2A.Z is the result of a sequential cascade initiated by Tip60-mediated acetylation of H4, leading to the recruitment of p300 via its BD to acetylate H2A.Z. Alternatively, Tip60 and p300/CBP may acetylate H2A.Z directly through independent pathways (Figure 6A).

We provide biochemical evidence that the presence of acetylated H4 in the nucleosome can have impact on p300-mediated acetylation of H2A.Z, suggesting that these two marks are co-localized. It was previously shown by immunoprecipitation that H2A.Z nucleosomes are enriched for H4ac (Draker et al., 2012; Myers et al., 2006). Based on our analysis of ChIP-seq data, we found that H2A.Zac and H4ac co-occurred predominantly at promoters and enhancers. However, at a third of all enhancers, these marks did not co-occur. After dissecting the epigenetic features of each sub-group of enhancers, we propose a dynamic mechanism for enhancer activation through three states of activity (Figure 6B): poised, poised-active, and active. Each state has a preferential H4ac/H2A.Zac combination that would initiate from H4ac-marked nucleosomes at poised enhancers that enables the recruitment of p300 through its BD. This may trigger H2A.Z acetylation through p300 in a poised/active state and deacetylation of H4 in a fully enhancer-activated state.

Additionally, we also find different transcriptional features of each state. H2A.Zac-unique enhancers are enriched at intergenic regions or within lowly expressed genes; conversely, H4ac-unique enhancers are present in intragenic regions and are associated with highly transcribed genes, whereas common enhancers are characterized by an intermediate state regarding transcription elongation. The lack of H2A.Zac at intragenic enhancers of highly expressed genes could be due to the previously reported active removal of H2A.Z at gene bodies during transcription elongation (Hardy et al., 2009; Lashgari et al., 2017). It is therefore interesting to note that H2A.Zac-marked active enhancers are not present within the gene they activate, as transcription elongation of the gene would remove H2A.Z from the enhancer, suggesting that H2A.Zac enhancers are likely acting as trans-regulatory elements. In this regard, a recent study showed that functionally active intragenic enhancers can attenuate transcription of the host gene (Cinghu et al., 2017), supporting our observation.

In contrast, the lack of H4ac at H2A.Zac-unique enhancers is less clear. Genome-wide mapping of KATs and lysine deacetylases (KDACs) have shown that both enzyme families are targeted to active genes and correlate with transcription levels (Wang et al., 2009), which suggests a high turnover rate of histone acetylation at highly transcribed genes compared with lowly transcribed genes or intergenic regions. Weinert et al. data reported a higher deacetylation rate of H4 compared with H2A.Z (Weinert et al., 2018). We, therefore, propose that these different kinetics could partially explain the lack of H4ac at these H2A.Zac regions. However, we cannot rule out that p300 and Tip60 are able to acetylate H2A.Z without the presence of H4ac at these particular sites.

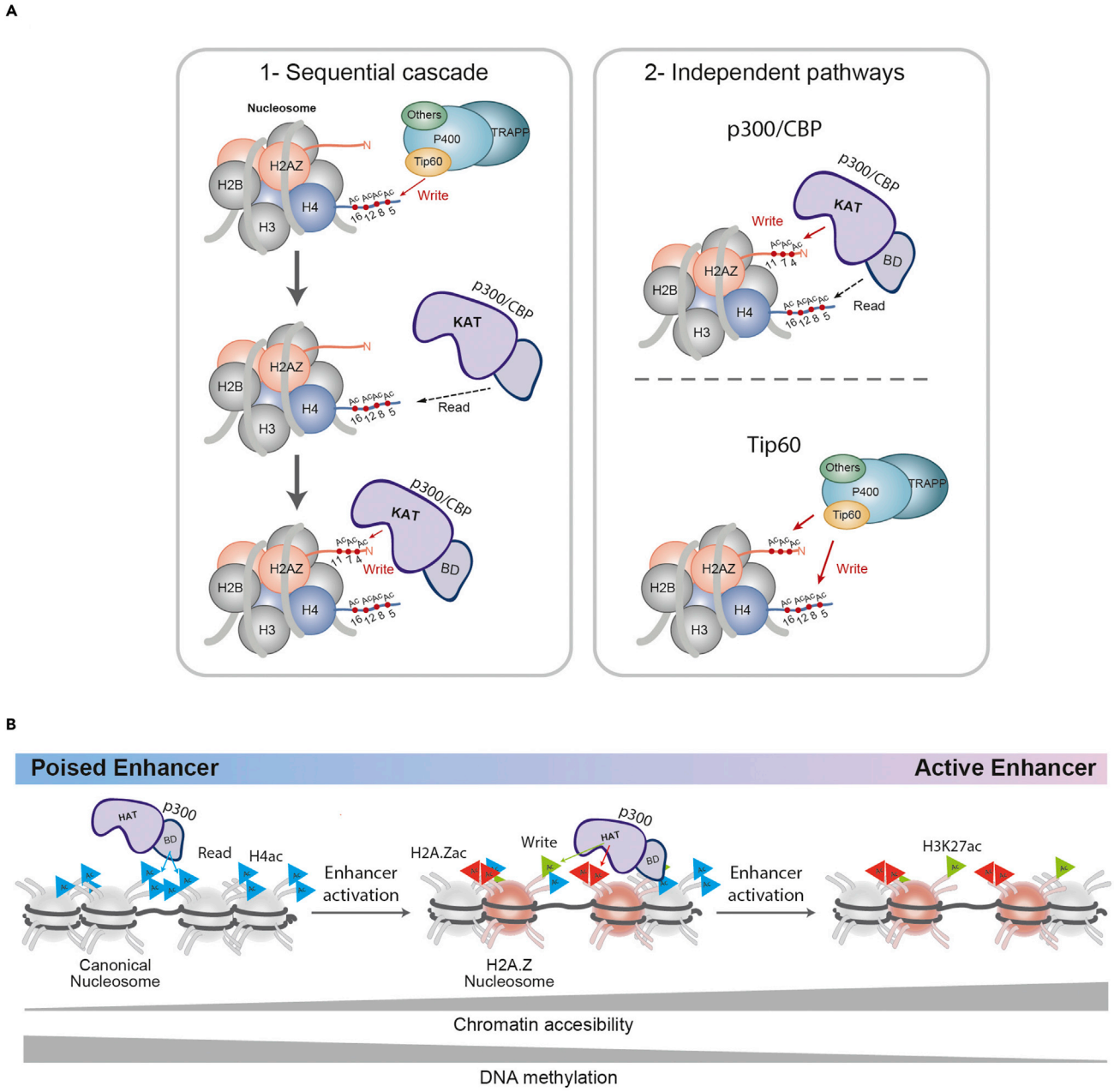

Figure 6. Model Figure of H2A.Z Acetylation Writing Mechanism

(A) Proposed models for Tip60- and p300-mediated acetylation of H2A.Z. (1) Sequential cascade: Tip60 acetylates H4, which drives recruitment of p300 and acetylation of H2A.Z. (2) Independent mechanisms: Tip60 directly targets acetylation of H2A.Z potentially during histone exchange and p300 acetylates H2A.Z at the chromatin to maintain nucleosomal acetylation.

(B) The combinatorial subgroups of H2A.Zac and H4ac at enhancers are snapshot of a dynamic mechanism for enhancer activation through three states: poised, poised-active, and active.

Collectively, we demonstrate that p300/CBP, complementary to Tip60, are essential KATs for the acetylation of H2A.Z, answering the long-standing question of what enzymes are responsible for this important modification. We reveal a mechanism of histone PTM crosstalk and define an enhancer code based on the patterning of H4ac and H2A.Zac. Both p300 and H2A.Z have been implicated in many human cancers (reviewed in Iyer et al., 2004; Vardabasso et al., 2014); therefore, this study provides p300 as an additional target for H2A.Zac-based chromatin therapy in cancer.

Limitations of the Study

In this study we demonstrate that p300-BD interaction with H4ac enhances H2A.Z acetylation using an inhibitor of p300 BD. However, we were not able to directly compare p300-mediated acetylation in a nucleosomal context with pre-installed H4ac/H2A.Z nucleosomes due to the technical difficulty in generating recombinant H4ac/H2A.Z combinatorial nucleosomes *in vitro*. Additionally, we found that H2A.Zac levels are reduced after inhibition of both Tip60 and p300, but we were unable in this study to determine if the mechanism that results in H2A.Zac involves a sequential cascade through H4ac or occurs through independent pathways. Future studies will focus on resolving the interplay and order of events that are associated with Tip60 and p300 in driving the acetylation of H2A.Z.

METHODS

All methods can be found in the accompanying Transparent Methods supplemental file.

SUPPLEMENTAL INFORMATION

Supplemental Information can be found online at https://doi.org/10.1016/j.isci.2019.10.053.

ACKNOWLEDGMENTS

We thank Dr. Ozren Bogdanovic and Dr. Paul Timpson for their review and feedback on the manuscript. This work was funded by National Health and Medical Research Council, Australia (NHMRC) project grant (#1144574) (S.J.C and F.V.M); National Institutes of Health, USA (NIH) project grant (R35GM124736) (S.B.R); NHMRC Fellowship (#1063559) (S.J.C.); Cancer Institute NSW Career Development fellowship (CDF181218, from 2019) (F.V.M); and UNSW Sydney University Tuition Fee Scholarship (TFS), Australia (Y.C.S.). We thank Epicypher, Inc. for gifting nucleosome reagents for this study.

AUTHOR CONTRIBUTIONS

Conception and design: Y.C.S., F.V.M., S.J.C., E.M.C., and S.B.R.; Biochemical experiments: E.M.C., Y.C.S., J.H., E.C.S., and R.M.V.; Mass-spec experiments: K.K. and E.M.C.; In-cell experiments: Y.C.S., D.M., and G.C.S; NGS analysis: Y.C.S.; Interpretation of the data: Y.C.S., F.V.M., S.J.C., E.M.C., and S.B.R.; Writing and review of manuscript Y.C.S., F.V.M., S.J.C., E.M.C., R.M.V., and S.B.R.. All authors have read and approved the final manuscript.

DECLARATION OF INTERESTS

S.B.R. has served in a compensated consulting role for EpiCypher, Inc. All other authors declare no competing interest.

Received: March 22, 2019
Revised: September 20, 2019
Accepted: October 24, 2019
Published: November 22, 2019

REFERENCES

Altaf, M., Auger, A., Monnet-Saksouk, J., Brodeur, J., Piquet, S., Cramet, M., Bouchard, N., Lacoste, N., Utley, R.T., Gaudreau, L., et al. (2010). NuA4-dependent acetylation of nucleosomal histones H4 and H2A directly stimulates incorporation of H2A.Z by the SWR1 complex. J. Biol. Chem. *285*, 15966–15977.

Bellucci, L., Dalvai, M., Kocanova, S., Moutahir, F., and Bystricky, K. (2013). Activation of p21 by HDAC inhibitors requires acetylation of H2A.Z. PLoS One *8*, e54102.

Bruce, Myers, Mantouvalou, Lefevre, Greaves, Bonifer, Tremethick, Thorne, and Crane-Robinson. (2005). The replacement histone H2A.Z in a hyperacetylated form is a feature of active genes in the chicken. Nucleic Acids Res *33*, 5633–5639.

Brunelle, Nordell Markovits, Rodrigue, Lupien, Jacques, and Gevry. (2015). The histone variant H2A.Z is an important regulator of enhancer activity. Nucleic Acids Res *43*, 9742–9756.

Cai, Y., Jin, J., Tomomori-Sato, C., Sato, S., Sorokina, I., Parmely, T.J., Conaway, R.C., and Conaway, J.W. (2003). Identification of new subunits of the multiprotein mammalian TRRAP/TIP60-containing histone acetyltransferase complex. J. Biol. Chem. *278*, 42733–42736.

Choi, J., Heo, K., and An, W. (2009). Cooperative action of TIP48 and TIP49 in H2A.Z exchange catalyzed by acetylation of nucleosomal H2A. Nucleic Acids Res. *37*, 5993–6007.

Cinghu, S., Yang, P., Kosak, J.P., Conway, A.E., Kumar, D., Oldfield, A.J., Adelman, K., and Jothi, R. (2017). Intragenic enhancers attenuate host gene expression. Mol. Cell *68*, 104–117.e6.

Colino-Sanguino, Y., Clark, S.J., and Valdes-Mora, F. (2016). H2A.Z acetylation and transcription: ready, steady, go! Epigenomics *8*, 583–586.

Conery, A.R., Centore, R.C., Neiss, A., Keller, P.J., Joshi, S., Spillane, K.L., Sandy, P., Hatton, C., Pardo, E., Zawadzke, L., et al. (2016). Bromodomain inhibition of the transcriptional coactivators CBP/EP300 as a therapeutic strategy

to target the IRF4 network in multiple myeloma. Elife *5*, e10483.

Cornett, E.M., Dickson, B.M., Vaughan, R.M., Krishnan, S., Trievel, R.C., Strahl, B.D., and Rothbart, S.B. (2016). Substrate specificity profiling of histone-modifying enzymes by peptide microarray. Methods Enzymol. *574*, 31–52.

Corujo, D., and Buschbeck, M. (2018). Post-Translational modifications of H2A histone variants and their role in cancer. Cancers (Basel) *10*, 59.

Creyghton, M.P., Cheng, A.W., Welstead, G.G., Kooistra, T., Carey, B.W., Steine, E.J., Hanna, J., Lodato, M.A., Frampton, G.M., Sharp, P.A., et al. (2010). Histone H3K27ac separates active from poised enhancers and predicts developmental state. Proc. Natl. Acad. Sci. U S A *107*, 21931–21936.

Dalvai, M., Bellucci, L., Fleury, L., Lavigne, A.C., Moutahir, F., and Bystricky, K. (2012). H2A.Z-dependent crosstalk between enhancer and promoter regulates Cyclin D1 expression. Oncogene *32*, 4243–4251.

Dalvai, M., Fleury, L., Bellucci, L., Kocanova, S., and Bystricky, K. (2013). TIP48/Reptin and H2A.Z requirement for initiating chromatin remodeling in estrogen-activated transcription. PLoS Genet. *9*, e1003387.

Dancy, B.M., and Cole, P.A. (2015). Protein lysine acetylation by p300/CBP. Chem. Rev. *115*, 2419–2452.

Delvecchio, M., Gaucher, J., Aguilar-Gurrieri, C., Ortega, E., and Panne, D. (2013). Structure of the p300 catalytic core and implications for chromatin targeting and HAT regulation. Nat. Struct. Mol. Biol. *20*, 1040–1046.

Dickson, B.M., Cornett, E.M., Ramjan, Z., and Rothbart, S.B. (2016). ArrayNinja: an open source platform for unified planning and analysis of microarray experiments. Methods Enzymol. *574*, 53–77.

Doyon, Y., Selleck, W., Lane, W.S., Tan, S., and Cote, J. (2004). Structural and functional conservation of the NuA4 histone acetyltransferase complex from yeast to humans. Mol. Cell Biol. *24*, 1884–1896.

Draker, R., Ng, M.K., Sarcinella, E., Ignatchenko, V., Kislinger, T., and Cheung, P. (2012). A combination of H2A.Z and H4 acetylation recruits Brd2 to chromatin during transcriptional activation. PLoS Genet. *8*, e1003047.

Dryhurst, D., Ishibashi, T., Rose, K.L., Eirin-Lopez, J.M., McDonald, D., Silva-Moreno, B., Veldhoen, N., Helbing, C.C., Hendzel, M.J., Shabanowitz, J., et al. (2009). Characterization of the histone H2A.Z-1 and H2A.Z-2 isoforms in vertebrates. BMC Biol. *7*, 86.

Dryhurst, McMullen, Fazli, Rennie, and Ausio. (2012). Histone H2A.Z prepares the prostate specific antigen (PSA) gene for androgen receptor-mediated transcription and is upregulated in a model of prostate cancer progression. Cancer Lett *315*, 38–47.

Ernst, and Kellis. (2012). ChromHMM: automating chromatin-state discovery and characterization. Nat Methods *9*, 215–216.

Giaimo, B.D., Ferrante, F., Herchenrother, A., Hake, S.B., and Borggrefe, T. (2019). The histone variant H2A.Z in gene regulation. Epigenetics Chromatin. *12*, 37.

Giaimo, B.D., Ferrante, F., Vallejo, D.M., Hein, K., Gutierrez-Perez, I., Nist, A., Stiewe, T., Mittler, G., Herold, S., Zimmermann, T., et al. (2018). Histone variant H2A.Z deposition and acetylation directs the canonical Notch signaling response. Nucleic Acids Res. *46*, 8197–8215.

Halley, Kaplan, Wang, Kobor, and Rine. (2010). Roles for H2A.Z and Its Acetylation in GAL1 Transcription and Gene Induction, but Not GAL1-Transcriptional Memory. PLoS Biol *8*, e1000401.

Hammitzsch, A., Tallant, C., Fedorov, O., O'Mahony, A., Brennan, P.E., Hay, D.A., Martinez, F.O., Al-Mossawi, M.H., de Wit, J., Vecellio, M., et al. (2015). CBP30, a selective CBP/p300 bromodomain inhibitor, suppresses human Th17 responses. Proc. Natl. Acad. Sci. U S A *112*, 10768–10773.

Hardy, S., Jacques, P.E., Gevry, N., Forest, A., Fortin, M.E., Laflamme, L., Gaudreau, L., and Robert, F. (2009). The euchromatic and heterochromatic landscapes are shaped by antagonizing effects of transcription on H2A.Z deposition. PLoS Genet. *5*, e1000687.

Hilton, I.B., D'Ippolito, A.M., Vockley, C.M., Thakore, P.I., Crawford, G.E., Reddy, T.E., and Gersbach, C.A. (2015). Epigenome editing by a CRISPR-Cas9-based acetyltransferase activates genes from promoters and enhancers. Nat. Biotechnol. *33*, 510–517.

Hu, G., Cui, K., Northrup, D., Liu, C., Wang, C., Tang, Q., Ge, K., Levens, D., Crane-Robinson, C., and Zhao, K. (2013). H2A.Z facilitates access of active and repressive complexes to chromatin in embryonic stem cell self-renewal and differentiation. Cell Stem Cell *12*, 180–192.

Ishibashi, T., Dryhurst, D., Rose, K.L., Shabanowitz, J., Hunt, D.F., and Ausio, J. (2009). Acetylation of vertebrate H2A.Z and its effect on the structure of the nucleosome. Biochemistry *48*, 5007–5017.

Ito, T., Ikehara, T., Nakagawa, T., Kraus, W.L., and Muramatsu, M. (2000). p300-mediated acetylation facilitates the transfer of histone H2A-H2B dimers from nucleosomes to a histone chaperone. Genes Dev. *14*, 1899–1907.

Ito, S., Kayukawa, N., Ueda, T., Taniguchi, H., Morioka, Y., Hongo, F., and Ukimura, O. (2018). MRGBP promotes AR-mediated transactivation of KLK3 and TMPRSS2 via acetylation of histone H2A.Z in prostate cancer cells. Biochim. Biophys. Acta Gene Regul. Mech. *1861*, 794–802.

Iyer, N.G., Ozdag, H., and Caldas, C. (2004). p300/CBP and cancer. Oncogene *23*, 4225–4231.

Jeong, K.W., Kim, K., Situ, A.J., Ulmer, T.S., An, W., and Stallcup, M.R. (2011). Recognition of enhancer element-specific histone methylation by TIP60 in transcriptional activation. Nat. Struct. Mol. Biol. *18*, 1358–1365.

Jin, Yu, Wang, Zhang, Kasper, Lee, Wang, Brindle, Dent, and Ge. (2011). Distinct roles of GCN5/PCAF-mediated H3K9ac and CBP/p300-mediated H3K18/27ac in nuclear receptor transactivation. EMBO J *30*, 249–262.

Kamakaka, and Biggins. (2005). Histone variants: deviants? Genes Dev *19*, 295–310.

Kelly, T.K., Liu, Y., Lay, F.D., Liang, G., Berman, B.P., and Jones, P.A. (2012). Genome-wide mapping of nucleosome positioning and DNA methylation within individual DNA molecules. Genome Res. *22*, 2497–2506.

Keogh, M.C., Mennella, T.A., Sawa, C., Berthelet, S., Krogan, N.J., Wolek, A., Podolny, V., Carpenter, L.R., Greenblatt, J.F., Baetz, K., et al. (2006). The Saccharomyces cerevisiae histone H2A variant Htz1 is acetylated by NuA4. Genes Dev. *20*, 660–665.

Kim, T.K., Hemberg, M., Gray, J.M., Costa, A.M., Bear, D.M., Wu, J., Harmin, D.A., Laptewicz, M., Barbara-Haley, K., Kuersten, S., et al. (2010). Widespread transcription at neuronal activity-regulated enhancers. Nature *465*, 182–187.

Kimura, and Horikoshi. (1998). Tip60 acetylates six lysines of a specific class in core histones in vitro. Genes Cells *3*, 789–800.

Ku, Jaffe, Koche, Rheinbay, Endoh, Koseki, Carr, and Bernstein. (2012). H2A.Z landscapes and dual modifications in pluripotent and multipotent stem cells underlie complex genome regulatory functions. Genome Biol *13*, R85.

Kusch, T., Florens, L., Macdonald, W.H., Swanson, S.K., Glaser, R.L., Yates, J.R., 3rd, Abmayr, S.M., Washburn, M.P., and Workman, J.L. (2004). Acetylation by Tip60 is required for selective histone variant exchange at DNA lesions. Science *306*, 2084–2087.

Lashgari, A., Millau, J.F., Jacques, P.E., and Gaudreau, L. (2017). Global inhibition of transcription causes an increase in histone H2A.Z incorporation within gene bodies. Nucleic Acids Res. *45*, 12715–12722.

Lasko, L.M., Jakob, C.G., Edalji, R.P., Qiu, W., Montgomery, D., Digiammarino, E.L., Hansen, T.M., Risi, R.M., Frey, R., Manaves, V., et al. (2017). Discovery of a selective catalytic p300/CBP inhibitor that targets lineage-specific tumours. Nature *550*, 128–132.

Li, M.L., Jiang, Q., Bhanu, N.V., Wu, J., Li, W., Garcia, B.A., and Greenberg, R.A. (2019). Phosphorylation of TIP60 suppresses 53BP1 localization at DNA damage sites. Mol. Cell Biol. *39*, e00209–18.

Link, S., Spitzer, R.M.M., Sana, M., Torrado, M., Volker-Albert, M.C., Keilhauer, E.C., Burgold, T., Punzeler, S., Low, J.K.K., Lindstrom, I., et al. (2018). PWWP2A binds distinct chromatin moieties and interacts with an MTA1-specific core NuRD complex. Nat. Commun. *9*, 4300.

Liu, X., Wang, L., Zhao, K., Thompson, P.R., Hwang, Y., Marmorstein, R., and Cole, P.A. (2008). The structural basis of protein acetylation by the p300/CBP transcriptional coactivator. Nature *451*, 846–850.

Manning, E.T., Ikehara, T., Ito, T., Kadonaga, J.T., and Kraus, W.L. (2001). p300 forms a stable,

template-committed complex with chromatin: role for the bromodomain. Mol. Cell Biol. *21*, 3876–3887.

Millar, C.B., Xu, F., Zhang, K., and Grunstein, M. (2006). Acetylation of H2AZ Lys 14 is associated with genome-wide gene activity in yeast. Genes Dev. *20*, 711–722.

Myers, F.A., Lefevre, P., Mantouvalou, E., Bruce, K., Lacroix, C., Bonifer, C., Thorne, A.W., and Crane-Robinson, C. (2006). Developmental activation of the lysozyme gene in chicken macrophage cells is linked to core histone acetylation at its enhancer elements. Nucleic Acids Res. *34*, 4025–4035.

Narkaj, K., Stefanelli, G., Wahdan, M., Azam, A.B., Ramzan, F., Steininger, C.F.D., Jr., Walters, B.J., and Zovkic, I.B. (2018). Blocking H2A.Z incorporation via Tip60 inhibition promotes systems consolidation of fear memory in mice. eNeuro *5*, 1.

Nguyen, U.T., Bittova, L., Muller, M.M., Fierz, B., David, Y., Houck-Loomis, B., Feng, V., Dann, G.P., and Muir, T.W. (2014). Accelerated chromatin biochemistry using DNA-barcoded nucleosome libraries. Nat. Methods *11*, 834–840.

Obri, A., Ouararhni, K., Papin, C., Diebold, M.L., Padmanabhan, K., Marek, M., Stoll, I., Roy, L., Reilly, P.T., Mak, T.W., et al. (2014). ANP32E is a histone chaperone that removes H2A.Z from chromatin. Nature *505*, 648–653.

Ogryzko, V.V., Schiltz, R.L., Russanova, V., Howard, B.H., and Nakatani, Y. (1996). The transcriptional coactivators p300 and CBP are histone acetyltransferases. Cell *87*, 953–959.

Raisner, R., Kharbanda, S., Jin, L., Jeng, E., Chan, E., Merchant, M., Haverty, P.M., Bainer, R., Cheung, T., Arnott, D., et al. (2018). Enhancer activity requires CBP/P300 bromodomain-dependent histone H3K27 acetylation. Cell Rep. *24*, 1722–1729.

Rothbart, S.B., Dickson, B.M., Raab, J.R., Grzybowski, A.T., Krajewski, K., Guo, A.H., Shanle, E.K., Josefowicz, S.Z., Fuchs, S.M., Allis, C.D., et al. (2015). An interactive database for the assessment of histone antibody specificity. Mol. Cell *59*, 502–511.

Rothbart, S.B., Krajewski, K., Strahl, B.D., and Fuchs, S.M. (2012a). Peptide microarrays to interrogate the "histone code". Methods Enzymol. *512*, 107–135.

Rothbart, S.B., Lin, S., Britton, L.M., Krajewski, K., Keogh, M.C., Garcia, B.A., and Strahl, B.D. (2012b). Poly-acetylated chromatin signatures are preferred epitopes for site-specific histone H4 acetyl antibodies. Sci. Rep. *2*, 489.

Schiltz, R.L., Mizzen, C.A., Vassilev, A., Cook, R.G., Allis, C.D., and Nakatani, Y. (1999). Overlapping but distinct patterns of histone acetylation by the human coactivators p300 and PCAF within nucleosomal substrates. J. Biol. Chem. *274*, 1189–1192.

Semer, M., Bidon, B., Larnicol, A., Caliskan, G., Catez, P., Egly, J.M., Coin, F., and Le May, N. (2019). DNA repair complex licenses acetylation of H2A.Z.1 by KAT2A during transcription. Nat. Chem. Biol. *15*, 992–1000.

Sevilla, A., and Binda, O. (2014). Post-translational modifications of the histone variant H2AZ. Stem Cell Res. *12*, 289–295.

Suto, R.K., Clarkson, M.J., Tremethick, D.J., and Luger, K. (2000). Crystal structure of a nucleosome core particle containing the variant histone H2A.Z. Nat. Struct. Biol. *7*, 1121–1124.

Valdes-Mora, F., Gould, C.M., Colino-Sanguino, Y., Qu, W., Song, J.Z., Taylor, K.M., Buske, F.A., Statham, A.L., Nair, S.S., Armstrong, N.J., et al. (2017). Acetylated histone variant H2A.Z is involved in the activation of neo-enhancers in prostate cancer. Nat. Commun. *8*, 1346.

Valdes-Mora, Song, Statham, Strbenac, Robinson, Nair, Patterson, Tremethick, Stirzaker, and Clark. (2012). Acetylation of H2A.Z is a key epigenetic modification associated with gene deregulation and epigenetic remodeling in cancer. Genome Res *22*, 307–321.

Vardabasso, C., Gaspar-Maia, A., Hasson, D., Punzeler, S., Valle-Garcia, D., Straub, T., Keilhauer, E.C., Strub, T., Dong, J., Panda, T., et al. (2015). Histone variant H2A.Z.2 mediates proliferation and drug sensitivity of malignant melanoma. Mol. Cell *59*, 75–88.

Vardabasso, C., Hasson, D., Ratnakumar, K., Chung, C.Y., Duarte, L.F., and Bernstein, E. (2014). Histone variants: emerging players in cancer biology. Cell Mol. Life Sci. *71*, 379–404.

Voss, A.K., and Thomas, T. (2018). Histone lysine and genomic targets of histone acetyltransferases in mammals. Bioessays *40*, e1800078.

Wang, Z., Zang, C., Cui, K., Schones, D.E., Barski, A., Peng, W., and Zhao, K. (2009). Genome-wide mapping of HATs and HDACs reveals distinct functions in active and inactive genes. Cell *138*, 1019–1031.

Weinert, B.T., Narita, T., Satpathy, S., Srinivasan, B., Hansen, B.K., Scholz, C., Hamilton, W.B., Zucconi, B.E., Wang, W.W., Liu, W.R., et al. (2018). Time-resolved analysis reveals rapid dynamics and broad scope of the CBP/p300 acetylome. Cell *174*, 231–244.e12.

Yang, C., Wu, J., and Zheng, Y.G. (2012). Function of the active site lysine autoacetylation in Tip60 catalysis. PLoS One *7*, e32886.

Zeng, L., Zhang, Q., Gerona-Navarro, G., Moshkina, N., and Zhou, M.M. (2008). Structural basis of site-specific histone recognition by the bromodomains of human coactivators PCAF and CBP/p300. Structure *16*, 643–652.

Zlatanova, and Thakar. (2008). H2A.Z: view from the top. Structure *16*, 166–179.

ISCI, Volume *21*

Supplemental Information

A Read/Write Mechanism Connects p300 Bromodomain Function to H2A.Z Acetylation

Yolanda Colino-Sanguino, Evan M. Cornett, David Moulder, Grady C. Smith, Joel Hrit, Eric Cordeiro-Spinetti, Robert M. Vaughan, Krzysztof Krajewski, Scott B. Rothbart, Susan J. Clark, and Fátima Valdés-Mora

Supplemental Figures

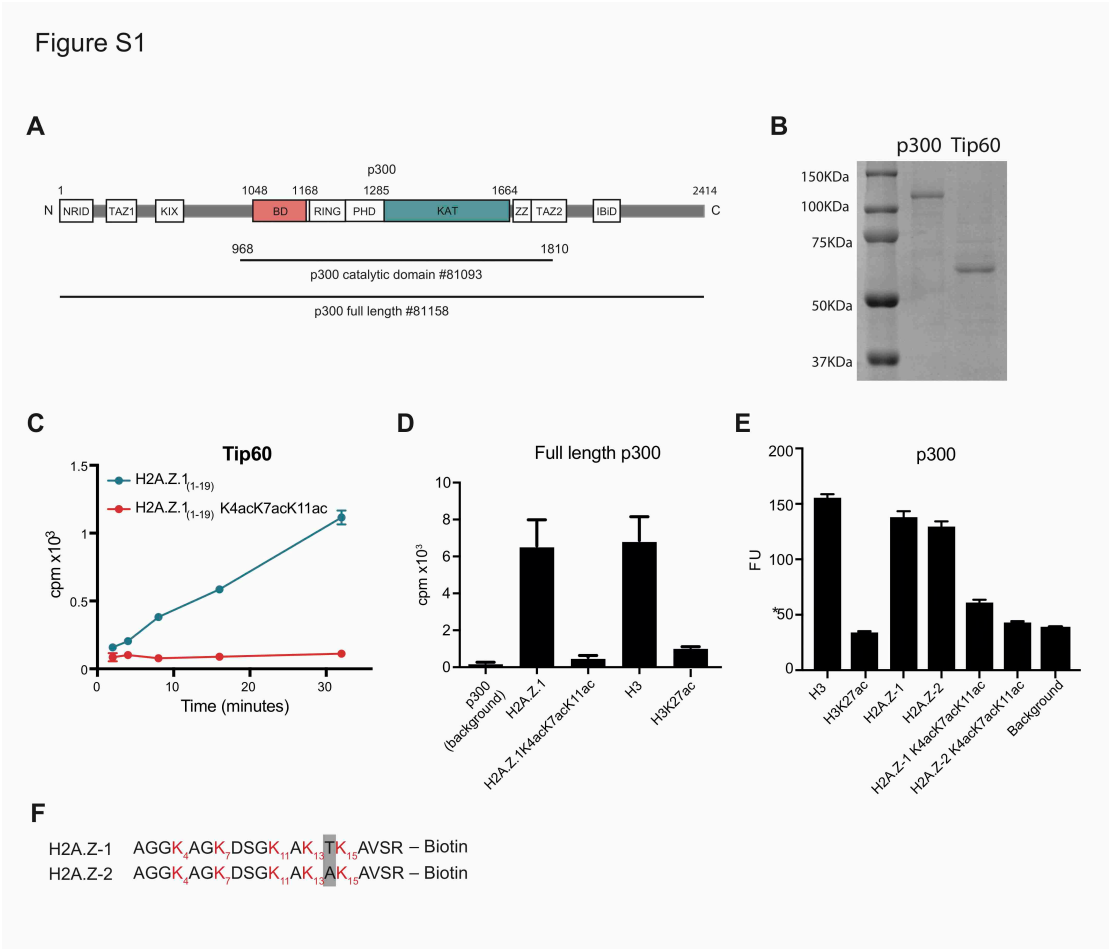

Figure S1. **Extended data for *in vitro* assays and explanatory diagrams.** Related to Figure 1. **(A)** p300 domain structure map and length information of the recombinant p300 enzymes used. **(B)** Coomassie staining of recombinant Tip60 and p300 catalytic domain used for the KAT assays. **(C)** In-solution H^3-Acetyl-CoA (AcCoA) assays measuring Tip60 activity as a function of time on the un-acetylated H2A.Z peptide (amino acid 1-19, H2A.Z-1 $_{(1-19)}$) and the tri-acetylated H2AZ at lysines 4, 7 and 11 (H2A.Z-1 $_{(1-19)}$K4acK7acK11ac). Same data as Figure 1B is shown but the scale of the y-axis has been adjusted to lower numbers to appreciate the discrete changes in H2A.Z acetylation. Data points are presented as counts per minute (cpm). Error bars represent the standard deviation from two measurements. **(D)** In-solution H^3-AcCoA KAT assays measuring full length p300 activity on the listed histone peptide substrates after 30 minutes of H^3-AcCoA incubation. Data points are presented as counts per minute (cpm). Error bars represent the standard deviation from two measurements. **(E)** Fluorescence assay measuring p300 activity on the listed histone peptide substrates after 15min incubation with Acetyl-CoA. Data points are presented as fluorescence units (FU). Error bars represent the standard deviation from two measurements. **(F)** Amino acid sequence of the isoforms H2A.Z-1 and H2A.Z-2 N-terminal peptides.

Figure S2

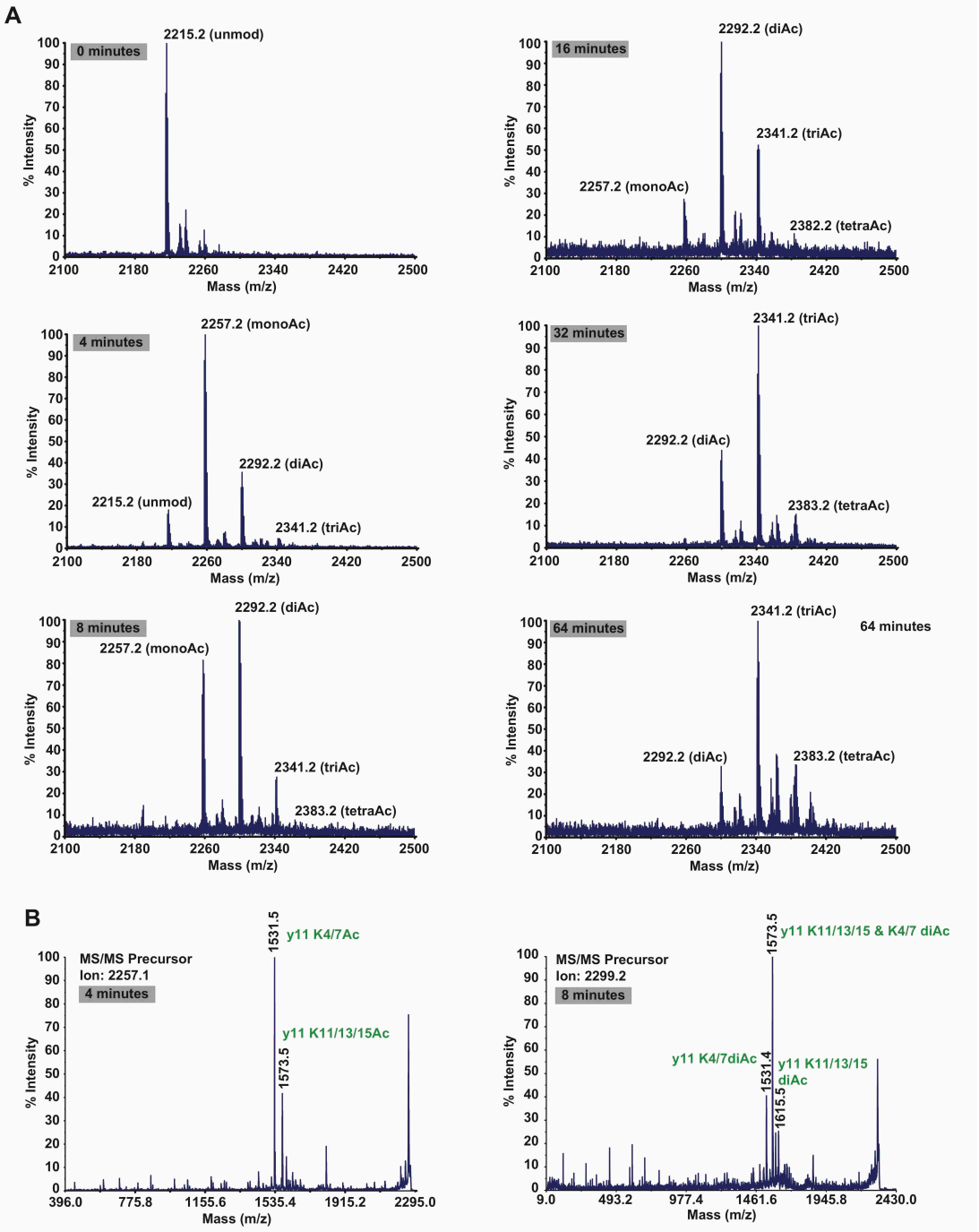

Figure S2. Mass spectrum of H2A.Z acetylated peptides. Related to Figure 1F **(A)** Time-course mass spectrometry (MS) analysis of p300-H2A.Z peptide reactions from Figure 1B. **(B)** Tandem-MS analysis of the mono and di-acetyl products at 4 and 8 minutes, respectively.

Figure S3

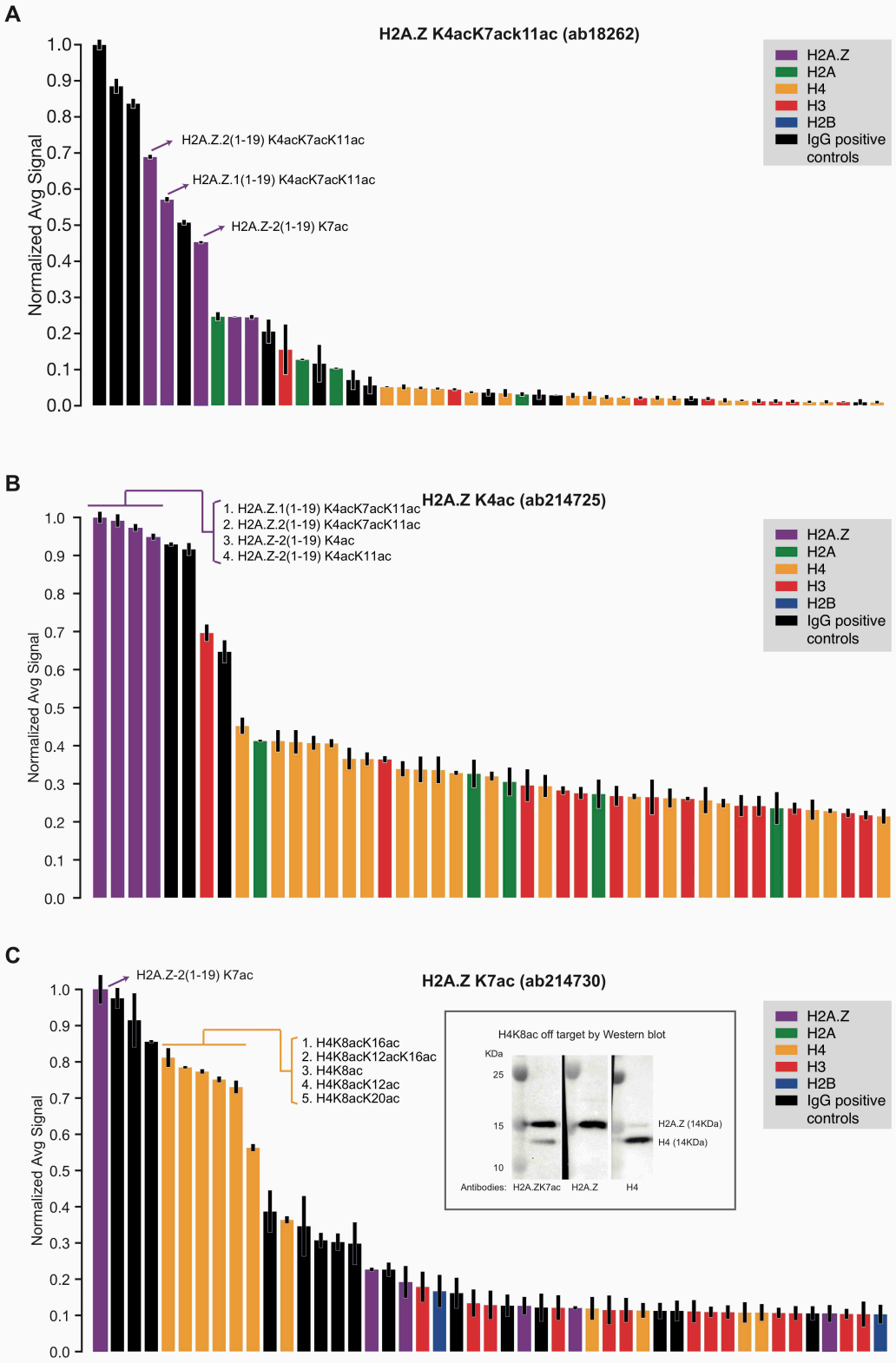

Figure S3. Antibody validation using histone peptide microarray. Related to Figure 2. Bar plots representing histone peptide microarrays hybridized with **(A)** H2A.Z K4acK7ack11ac antibody (ab18262), **(B)** H2A.ZK4ac (ab214725) and **(C)** H2A.ZK7ac (ab214730). Data are represented as mean +/- SEM (n=6). The inlet in Figure 3C shows the double band detected with the H2A.ZK7ac antibody by western blot imaging. For comparison, we also show images

from total H2A.Z and H4. The signal intensity of two arrays was averaged and normalized to the peptide with the strongest signal in each array. Array 2 was used for those experiments See list of peptides in Supplemental Table 1.

Figure S4

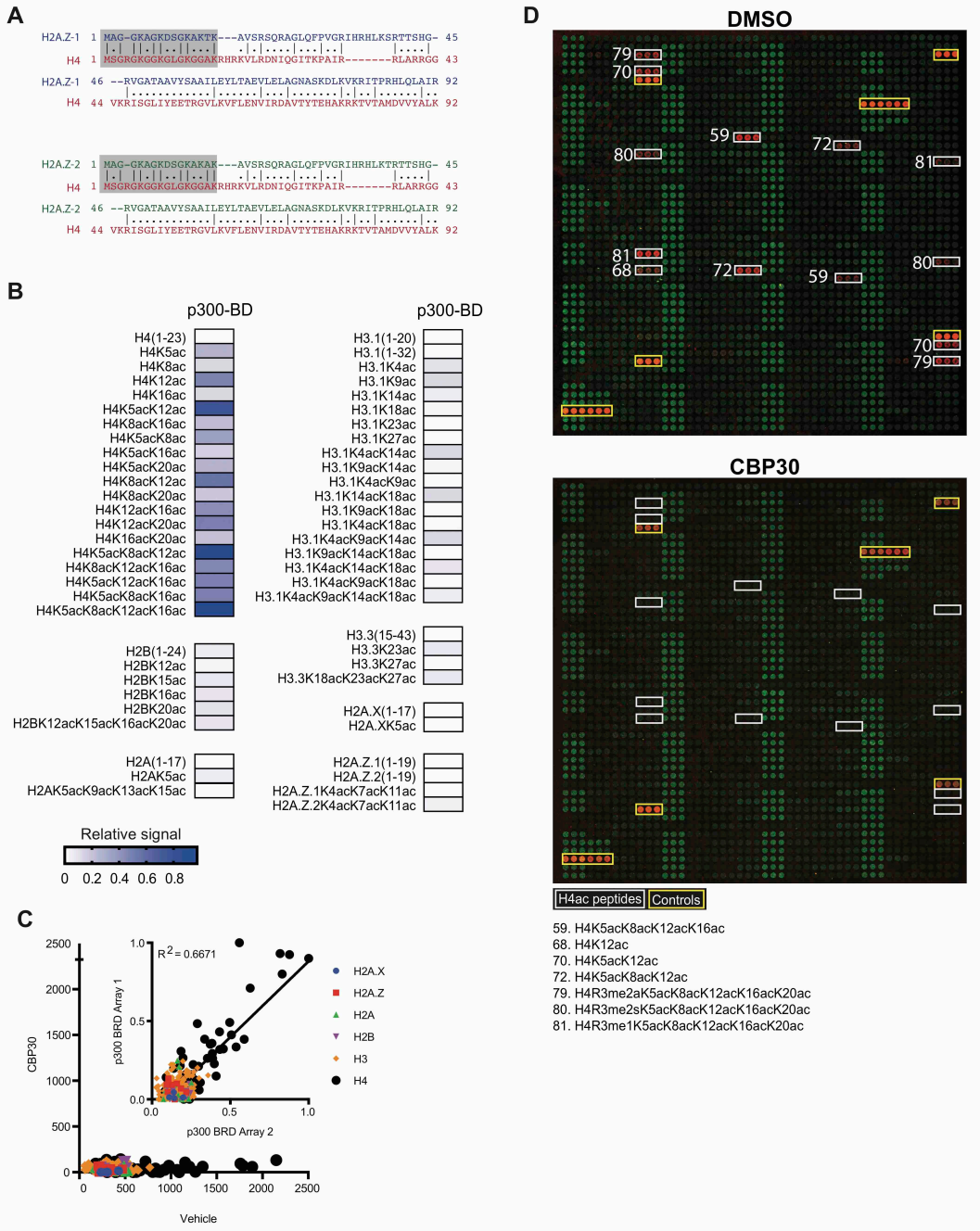

Figure S4. **Pair-wise alignment and extended representation of histone peptide array experiments.** Related to Figure 3. **(A)** Pairwise sequence alignment using the Smith-Waterman algorithm of H2A.Z-1 and H4. Matching amino acids have a mark-up line between them and the grey area delineates the matching lysines at the N-terminus. **(B)** Heatmap showing p300 BD binding to all acetylated histone peptides on the peptide microarray. The scalebar shows the color key of the relative intensity normalized to the peptide with the highest signal (H4K5acK8acK12acK16ac). Data are represented as mean normalized signal (n=6) **(C)** Scatterplots showing histone peptide microarray raw signal of each peptide hybridized with p300 BD in the presence of CBP30 inhibitor or the vehicle control, DMSO (outset). Comparison of two independent microarray experiments for the p300 BD (inset). Data are represented as mean raw signal (n=6). We performed linear regression analysis derived from the average of 6 individual peptide spots printed by two different pins in two very different locations on the slide and r2 calculation shows the degree of similarity between two different subarrays. **(D)** Representative image of peptide arrays hybridized with p300 bromodomain in the presence of CBP30 inhibitor or the vehicle control, DMSO. White boxes

mark peptides bound by p300 bromodomain in the vehicle control and yellow boxes demarcate positive controls. The different numbers display the peptides of interest for this study. The Array 1 was used for experiments from panel B, C, and D. A complete list of peptides included in the histone peptide microarray is in Supplemental Table 1.

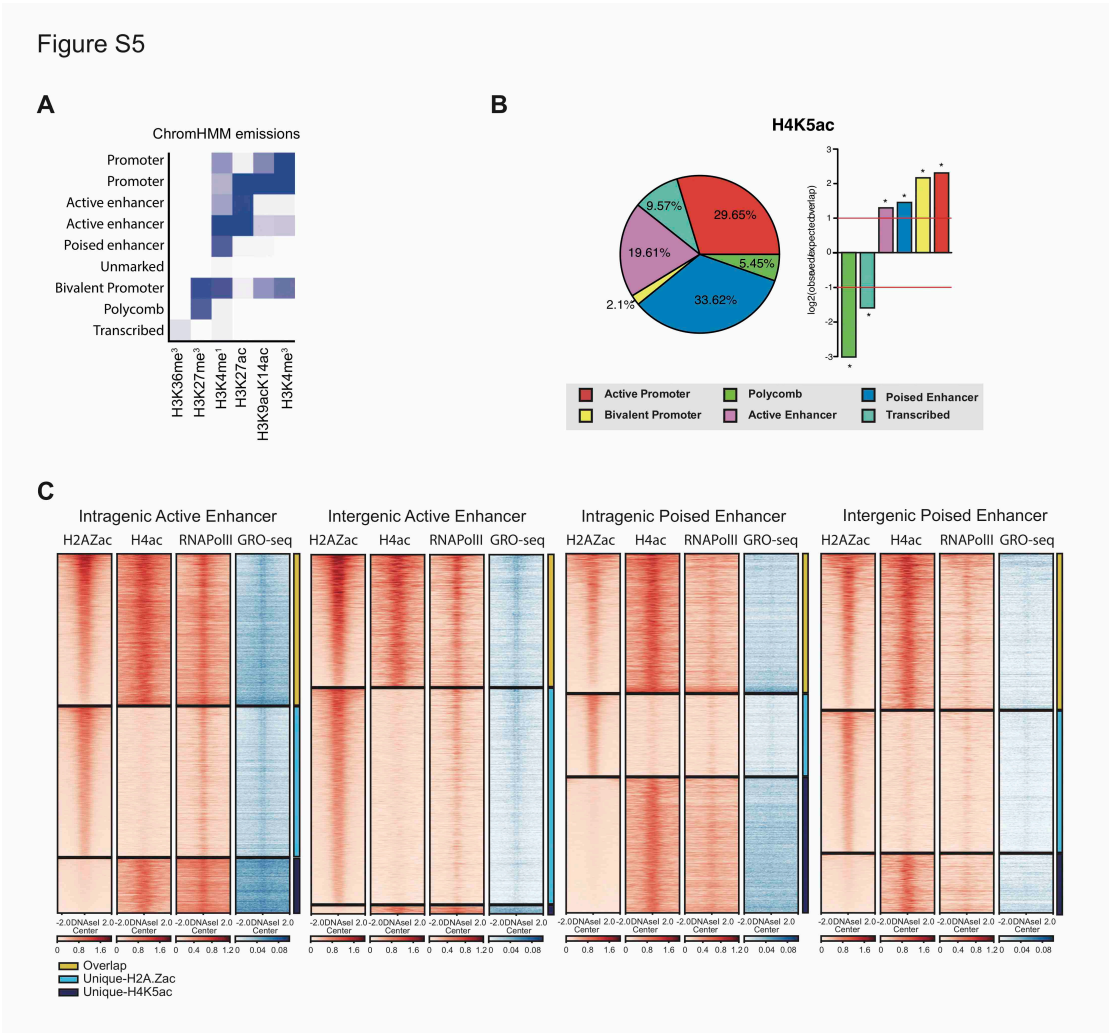

Figure S5. **Extended data for genomic analysis**. Related to Figure 4 and 5 **(A)** Heatmap of the ChromHMM state emissions from LNCaP cells. The x axis shows the different histone marks used for the partition of the genome in 9 chromatin states using the ChromHMM algorithm(Ernst and Kellis, 2012). The emission signal indicates the relative contribution of the histone mark in that state. Redundant states were merged into seven states and manually annotated by comparison to public ChromHMM states for HMEC cells (Ernst et al., 2011). **(B)** Genomic Association Test (GAT) of H4ac ChIP-seq peaks and ChromHMM regions in LNCaP cells. Pie charts representing the percentage of marked peaks falling in each ChromHMM state (left panel). Observed vs expected log fold enrichment graphs (right panel). *p< 0.0001. **(C)** Heatmaps showing H2A.Zac, H4ac, RNAPolII ChIP-seq and GRO-seq signal across active and poised enhancers further divided into intergenic and intragenic enhancers. Each enhancer is divided in three groups: H2A.Zac and H4ac common peaks (Common, yellow), H2A.Zac-unique peaks (H2A.Zac-unique, light blue) and H4ac-unique peaks (H4ac-unique, dark blue) and ordered based on H2A.Zac signal.

Supplemental Tables

Table S2: Datasets used in this publication. Related to Figure 4 and 5.

Target	Source	Company and Cat # Abs	Accession
ChIP-seq (H2A.Zac)	Valdes-Mora et al. Nature Communications 2017	Abcam ab18262	GSE76336
ChIP-seq (H2A.Z)	Valdes-Mora et al. Nature Communications 2017	Active Motif Cat #39113	GSE76336
ChIP-seq (H4K5ac)	Wang et al. Nature 2011	Upstate #07-327	GSE27823
ChIP-seq (p300)	Wang et al. Nature 2011	Santa Cruz #C-20	GSE27823
ChIP-seq (H3K4me3)	Bert et al., Cancer Cell 2013	Abcam ab8580	GSE38685
ChIP-seq (H3K27me3)	Bert et al., Cancer Cell 2013	Millipore #07-449	GSE38685
ChIP-seq (H3K4me1)	Taberlay et al., Genome Res 2016	Active Motif Cat # 39298	GSE73785
ChIP-seq (H3K27ac)	Taberlay et al., Genome Res 2016	Active Motif Cat #39133	GSE73785
ChIP-seq (H3K36me3)	Valdes-Mora et al. Nature Communications 2017	Abcam ab9050	GSE76336
ChIP-seq (H3ac)	Valdes-Mora et al. Nature Communications 2017	Millipore #06-599	GSE76336
ChIP-seq (Pol II phospho S5)	Tan et al., Mol Cell Biol 2012	Abcam, ab5131	GSE28264
NOMe-seq	Valdes-Mora et al. Nature Communications 2017		GSE76334
DNAseI-seq	ENCODE		GSE32970
RNA-seq	Taberlay et al., Genome Res 2016		GSE73785
GRO-seq	Puc et al., Cell 2015		GSE63202
ChromHMM	Valdes-Mora et al. Nature Communications 2017		GSE76337

Table S3. Small interfering RNA (siRNA) sequences. Related to Figure 2.

Gene target	Target sequence	Cat number
KAT5 (Tip60)	CGUAAGAACAAGAGUUAUU	J006301-08
KAT5 (Tip60)	AUGAAUGGGUGACGCAUGA	J006301-09
KAT5 (Tip60)	GGACAGCUCUGAUGGAAUA	J006301-10
KAT5 (Tip60)	GACCAAGUGUGACCUACGA	J006301-11
EP300 (p300)	GGACUACCCUAUCAAGUAA	J-003486-11
EP300 (p300)	GUUCAAUAAUGCCUGGUUA	J003486-13
EP300 (p300)	CGACAGGGAUGCAGCAACA	J003486-13
CREBBP(CBP)	GCACAGCCGUUUACCAUGA	J-003477-06
CREBBP(CBP)	UCACCAACGUGCCAAAUAU	J-003477-07
CREBBP(CBP)	GGGAUGAAGUCACGGUUUG	J-003477-08
CREBBP(CBP)	AAUAGUAACUCUGGCCAUA	J-003477-09

***** All siRNAs were ON-TARGET plus purchased from Dharmacon.

Table S4. Primer sequences. Related to Related to Figure 2.

Gene target	Primer sequence
KAT5_FW (Tip60)	GACCTACGACATCCTCCAGG
KAT5_ RV (Tip60)	CAGGTTCTGGGAATAACTCTTGT
EP300_FW (p300)	GCCGAGAATGTGGTGGAAC
EP300_RV (p300)	AGCCAAAATCTGTGCCATCG
CREBBP_FW (CBP)	TGACAGCACAGATTTTGGATCA
CREBBP_RV (CBP)	CGTAGAAGCTCCGACAGTTG
GAPDH_FW	CCACATCGCTCAGACACCAT
GAPDH_RV	ACCAGGCGCCCAATACG

* All primers were purchased from IDT.

Transparent Methods

Recombinant protein production
Bacterial expression constructs for the p300 bromodomain were transformed into Escherichia coli BL21(DE3) and grown in LB media (Caisson) at 37°C. When the OD600 (optical density at 600 nm) reached 0.6 to 0.8, the temperature was lowered to 16°C, isopropyl-β-d-thiogalactopyranoside (IPTG) was added (0.5 mM), and incubation was continued overnight with shaking. Bacteria were harvested by centrifugation and either frozen at −80°C or used immediately. Protein was purified with either glutathione agarose (GE Healthcare) according to the manufacturer's protocol.

In vitro peptide KAT assays
Reactions (10 µl) containing 1 µg of KAT, 1 µg of peptide substrate, and 1 µCi of H^3-AcCoA (PerkinElmer) in KAT reaction buffer (50 mM HEPES pH 7.5, 0.05% BSA) were incubated at room temperature as indicated. Reactions were stopped by adding trifluoracetic acid to a final concentration of 0.5%, neutralized by diluting with 135 µl of 50 mM NaHCO3, and transferred to streptavidin-coated FlashPlates (PerkinElmer). Plates were incubated for 15 min, sealed, and counted in a MicroBeta2 liquid scintillation counter (PerkinElmer) for 1 min per sample. The following KATs were used: Human recombinant p300 catalytic domain (Active Motif #31205), p300 full protein (Active Motif, #31124), Tip60 (Cayman Chemicals #10783). Histone peptide substrates were synthesized on PTI Symphony automated synthesizer using FMOC chemistry solid phase peptide synthesis. Fmoc group deprotection steps (2 x 7 min) were performed with 20% piperidine in N,N-dimethylformamide, coupling steps (2 x 20 min) were performed with 5 equivalents of Fmoc-amino acids and HATU coupling reagent, K(Ac) residues were introduced using Fmoc-Lys(Ac)-OH. After synthesis the peptides were cleaved from the resin by 2h treatment with 2.5% triisopropylsilane, 2.5% water in trifluoroacetic acid and precipitated with a cold diethyl ether. After precipitation the peptides were separated by centrifugation washed 3 x with cold ether, air dried, dissolved in 50% acetonitrile and lyophilized. Crude peptides were purified by a preparative reverse phase HPLC on Waters SymmetryShield RP18 column. The purified peptides were characterized using MALDI-TOF mass spectrometry and an analytical reverse phase HPLC.

In vitro nucleosomal KAT Assays
Reactions (10 µl) containing 1 µg of KAT, 1 µg of biotinylated recombinant nucleosome (EpiCypher: unmodified #16-006, H2A.Z.1 #16-0014, H2AZ.2 #16-0015, and H4 Tetraacetyl #16-0313), and 1 µCi of H^3-AcCoA (PerkinElmer) in KAT reaction buffer (50 mM HEPES pH 7.5, 0.05% BSA) were incubated at room temperature as indicated. Reactions were quenched by the addition of SDS loading buffer and resolved by SDS–polyacrylamide gel electrophoresis. Following the detection of total protein by Coomassie staining, gels were treated with EN3HANCE (PerkinElmer) and dried, and acetylated proteins were detected by autoradiography.

Fluorescence KAT assays
For the fluorescence KAT assay, recombinant human p300 (Active Motif #31205) and a commercial histone acetyltransferase kit (Active Motif # 56100) were used according the manufacture's instructions.

Histone peptide microarrays
Histone peptide microarrays were fabricated by depositing biotinylated histone peptides onto streptavidin-coated glass microscope slides using an Aushon 2470 microarray printer. Briefly, biotinylated peptides were deposited onto streptavidin-coated glass microscope slides using an Aushon 2470 microarray printer. Arrays were blocked for 30 min in cold array hybridization buffer (1× PBS pH 7.6, 0.1% Tween-20, 5% BSA (OmniPur, Fraction V) and GST-tagged proteins (1 µM) were hybridized to the microarray in a humidified chamber overnight at 4°C. Bound protein was labelled with α-GST primary (Sigma #7781) and AlexaFluor 647-conjugated secondary antibody (Invitrogen #A21245). Microarrays images were collected at 20 µm resolution using an Innoscan 1100AL microarray scanner (Innopsys). Image processing and data analysis was performed using ArrayNinja (Dickson et al., 2016). Each unique peptide feature (see Supplementary Table 1 for a full list of peptide features spotted on each array) was spotted in triplicate two times per subarray, and values presented are the

mean of measured signals for these individual peptide spots. Background was subtracted using reference spots with no peptides. Array data was normalized to the peptide with the strongest signal in the array or to an IgG control. Peptide arrays are now commercially available through EpiCypher (Catalog # 11-4001)

MALDI-TOF-MS analysis of KAT reactions

For MS experiments, reactions were performed as described above with one exception: H^3-AcCoA was replaced with final concentration of 500μM unlabelled AcCoA. Reactions were quenched with 0.5% trifluoroacetic acid at indicated timepoints, cleaned up using Pierce C18 Spin Columns (#89870), and analyzed by MS. KAT-reacted samples were deposited on a MALDI target plate (4 μl per spot) and mixed with 1 μl of matrix solution (α-cyano-4-hydroxycinnamic acid in 50% acetonitrile). MALDI-TOF-MS and MS/MS (positive ion mode at 1 kV) spectra were collected using SCIEX TOF/TOF 5800 MALDI MS spectrometer. The peptide fragmentation modeling and peak assignments were done using the Peptide Sequence Fragmentation Modeling tool (https://omics.pnl.gov/software/molecular-weight-calculator).

Cell lines, treatments and transfections

LNCaP prostate cancer cells (Cambrex Bio Science Cat. No. CC-2555) were cultured in RPMI 1640 media (Gibco, #11875-093) supplemented with foetal bovine serum (10%, hyclone #SH30084.03), 2mM L-glutamine (Gibco, #25030-081) and Penicillin/Streptomysin (1%, Gibco, #15070-063). HCT116 colorectal carcinoma cells were gifted by Stephen Baylin laboratory and were maintained in McCoy's 5A media (Gibco, #16600-082) supplemented with foetal bovine serum (10%, hyclone #SH30084.03) and Penicillin/Streptomysin (1%, Gibco, #15070-063). All cell lines were authenticated by STR profiling (CellBank Australia, Westmead, NSW, Australia) and cultured for <6 months after authentication. LNCaP and HCT116 cells were seeded at 70% confluence and were treated with A-485 0.08, 0.4, 2 or 10μM and the compound control A-486 and CBP30 1, 2, 5 and 10 μM for 24h. The untreated controls were mocked treated with the equivalent amount of the highest concentration of the vehicle used to dissolve the drugs, 100% dimethyl sulfoxide (DMSO). For siRNA transfections LNCaP cells were seeded at a density of 775,000 cells per 6cm dish. 24hrs post-seeding cells were transfected with 20nM of Dharmacon ON-TARGET plus pooled KAT5 siRNAs, EP300 and CREBBP siRNAs, or EP300, CREBBP and KAT5 siRNAs (listed in Supplemental Table 3) and 8μL Dharmafect 2, according to the manufacturer protocol. In parallel we also transfected cells with 20nM of Dharmacon ON-TARGET plus pooled Non-targeting siRNA (Scramble) as a control. Cells were harvested 72h post-transfection.

Chromatin extraction, western blot and antibodies

Asynchronously growing LNCaP and HCT116 cells were harvested by trypsinization 24 hr after treatment or 72hr after transfection. Pellets were washed once with cold 1x PBS, snap frozen in liquid N2 and either processed immediately or stored at −80°C. Cell pellets were resuspended in 1x volume CSK buffer (10 mM PIPES pH 7.0, 300 mM sucrose, 100 mM NaCl, 3 mM MgCl2, 0.1% Triton X-100 and 1x Complete EDTA-Free protease inhibitor cocktail from Roche) and incubated on ice for 1h. 10% of this total fraction was combined with an equivalent volume of CSK buffer complemented with Universal Nuclease (Thermo, 1:5,000). The remaining cell lysate was centrifuged at 1300 x g for 5 min at 4°C. The supernatant (soluble fraction) was collected. The chromatin pellet was resuspended in 1x volume CSK buffer and kept on ice for 10 min before being spun again at 1300 x g for 5 min at 4°C. The supernatant was discarded and the chromatin pellet was solubilized in Universal Nuclease-CSK buffer. Each protein fraction was quantified by Bradford Assay (BioRad), and 7.5 μg of protein from each fraction was resolved by SDS-PAGE, transferred to PVDF membrane (Thermo), and probed with the indicated antibodies. H2A.Ztri-ac (Abcam #18262; 1:500), H2A.ZK4ac (Abcam # 214725; 1:1000), H2A.ZK7ac (Abcam #214730; 1:1000), H2A.Z (Abcam #4174; 1:1000), H3k27ac (Active Motif #39133; 1:1000), H4tetra-ac (Millipore #05-1355;1:2000), H4 (Abcam #10158) and Tip60 (Santa Cruz, #166323, 1:500).
The specificity of the antibodies used for ChIP-seq is reported at http://www.histoneantibodies.com/

Fiji ImageJ software was used to quantify western blot images following the Gel Analysis method outlined in their documentation (Schindelin et al., 2012; Schneider et al., 2012).

Briefly, band densities were plotted using their Gels commands and area under the curve was quantified. Band densities of the protein of interest were divided by a loading control protein and further normalized to the control sample. Average and standard error of the mean were calculated for replicates using Prism 7 software and Student's t-test pairwise comparison was applied.

RNA extraction and real time qPCR

Total RNA extraction was performed using TRIzol reagent (Life Technologies, #15596018) following manufacturer's instructions. 10µg of extracted RNA were treated with Turbo DNA-free kit (ThermoFisher Scientific, #AM1907) and complementary DNA (cDNA) generation was performed using SuperScript III Reverse Transcriptase (Invitrogen, #18080-044) and random hexamer primers (ThermoFisher Scientific #SO142) following manufacturer's instructions. 3µL of diluted cDNA(1:10) was added to 7µL of PCR master mix containing, 5µL of Power Sybr Green (ThermoFisher Scientific, #4367659), 1µL of each primer set (2µM). Quantitative real-time PCR (qRT-PCR) was performed using the ABI-PRISM 7900HT Sequence Detection System using the following conditions: 1) 50^{o}C for 2 min; 2) 95^{o}C for 10 min; 3) 40 cycles of 95^{o}C for 15 sec and 60^{o}C for 1 min. The data is represented as the fold change of mRNA gene expression normalized to the endogenous reference *Gapdh* and relative to the scramble condition. The list of all primer sequences used for this manuscript can be found in Supplemental Table 4.

Data analysis:

ChIP-seq reads (see Supplemental Table 2) were mapped to the human genome (hg19) using Bowtie (version 1.0.1) (Langmead et al., 2009), allowing up to three mismatches. Non-uniquely alignable reads were excluded. For H2A.Zac and H4K5ac, broad peaks were called using PeakRanger (version 1.16) (Feng et al., 2011), peaks from replicates, when available, were combined by taking overlapping regions.

For Chromatin-state discovery and characterization, ChromHMM (Ernst and Kellis, 2012) was applied to ChIP aligned reads to partition the genome of LNCaP into 9 chromatin states. The following chromatin marks were used: H3K4Me3, H3ac, H3K4Me1, H3K27Me3, H3K36Me and H3K27ac (Table x). Redundant states were merged into seven distinct states and manually annotated based on the published ChromHMM model for HMEC cells (Ernst et al., 2011). To calculate the significance of overlap between H4K5ac and H2A.Zac or these two marks and ChromHMM states Genomic Association Tester (GAT) (Heger et al., 2013) was implemented using 100 permutation.

DeepTools2 was used to visualize ChIP-seq signal (Ramirez et al., 2016; Shen et al., 2014). Bigwig files were generated using "bamCoverage" function, reads were extended 300bp and normalized based on counts per million mapped read (CPM). Promoter heatmaps were centered on the TSS coordinates from RefSeq hg19 and enhancers were centered at DNaseI midpoints from ENCODE LNCaP data. Enhancers within 2kb of a TSS were discarded. Heatmap bin size was 10bp in a 4000bp window. In some analysis, active and poised enhancer bed files were divided into intragenic or intergenic based on their overlap with the Gencode transcript annotation (hg19).

NOMe-seq analysis were done as previously described (Statham et al., 2015; Taberlay et al., 2014; Valdes-Mora et al., 2017); briefly, raw reads were aligned to hg19 using bw-meth (Pedersen et al., 2014), PCR duplicates were removed and BisSNP v0.82.2 (Hu et al., 2013) was used to obtain methylation status of each WCG and GCH site in each sample. Next, data was transformed into a methylation counts and coverage table. To visualize and compare NOMe-seq profiles across enhancer groups the "methylationPlotRegion" was implemented from aaRon R package.

RNAseq data was processed as previously described (Taberlay et al., 2016), paired-end reads were trimmed using TrimGalore (version 0.11.2) and mapped to hg19 using STAR (version 2.4.0j)(Dobin et al., 2013). Mapped reads were counted into genes using RSEM (v1.3.0) and transcript per million (TPM) normalization was used. Box plots were performed using ggplot2 R package.

GRO-seq fastq files were aligned to hg19 using bowtie2 (version 2.2.4). Deeptools was used to plot normalized signal (CPM) as heatmaps and reads per bp per as profiles centered at the DNAseI midpoints.

Supplemental References

Cornett, E.M., Dickson, B.M., and Rothbart, S.B. (2017). Analysis of Histone Antibody Specificity with Peptide Microarrays. J Vis Exp.

Dickson, B.M., Cornett, E.M., Ramjan, Z., and Rothbart, S.B. (2016). ArrayNinja: An Open Source Platform for Unified Planning and Analysis of Microarray Experiments. Methods Enzymol *574*, 53-77.

Dobin, A., Davis, C.A., Schlesinger, F., Drenkow, J., Zaleski, C., Jha, S., Batut, P., Chaisson, M., and Gingeras, T.R. (2013). STAR: ultrafast universal RNA-seq aligner. Bioinformatics *29*, 15-21.

Ernst, J., and Kellis, M. (2012). ChromHMM: automating chromatin-state discovery and characterization. Nat Methods *9*, 215-216.

Ernst, J., Kheradpour, P., Mikkelsen, T.S., Shoresh, N., Ward, L.D., Epstein, C.B., Zhang, X., Wang, L., Issner, R., Coyne, M.*, et al.* (2011). Mapping and analysis of chromatin state dynamics in nine human cell types. Nature *473*, 43-49.

Feng, X., Grossman, R., and Stein, L. (2011). PeakRanger: a cloud-enabled peak caller for ChIP-seq data. BMC Bioinformatics *12*, 139.

Heger, A., Webber, C., Goodson, M., Ponting, C.P., and Lunter, G. (2013). GAT: a simulation framework for testing the association of genomic intervals. Bioinformatics *29*, 2046-2048.

Hu, G., Cui, K., Northrup, D., Liu, C., Wang, C., Tang, Q., Ge, K., Levens, D., Crane-Robinson, C., and Zhao, K. (2013). H2A.Z facilitates access of active and repressive complexes to chromatin in embryonic stem cell self-renewal and differentiation. Cell Stem Cell *12*, 180-192.

Langmead, B., Trapnell, C., Pop, M., and Salzberg, S.L. (2009). Ultrafast and memory-efficient alignment of short DNA sequences to the human genome. Genome Biol *10*, R25.

Pedersen, B.S., Eyring, K., De, S., Yang, I.V., and Schwartz, D.A. (2014). Fast and accurate alignment of long bisulfite-seq reads. arXiv:14011129 [qbioGN]

Ramirez, F., Ryan, D.P., Gruning, B., Bhardwaj, V., Kilpert, F., Richter, A.S., Heyne, S., Dundar, F., and Manke, T. (2016). deepTools2: a next generation web server for deep-sequencing data analysis. Nucleic Acids Res *44*, W160-165.

Schindelin, J., Arganda-Carreras, I., Frise, E., Kaynig, V., Longair, M., Pietzsch, T., Preibisch, S., Rueden, C., Saalfeld, S., Schmid, B.*, et al.* (2012). Fiji: an open-source platform for biological-image analysis. Nat Methods *9*, 676-682.

Schneider, C.A., Rasband, W.S., and Eliceiri, K.W. (2012). NIH Image to ImageJ: 25 years of image analysis. Nat Methods *9*, 671-675.

Shen, L., Shao, N., Liu, X., and Nestler, E. (2014). ngs.plot: Quick mining and visualization of next-generation sequencing data by integrating genomic databases. BMC Genomics *15*, 284.

Statham, A.L., Taberlay, P.C., Kelly, T.K., Jones, P.A., and Clark, S.J. (2015). Genome-wide nucleosome occupancy and DNA methylation profiling of four human cell lines. Genom Data *3*, 94-96.

Taberlay, P.C., Achinger-Kawecka, J., Lun, A.T., Buske, F.A., Sabir, K., Gould, C.M., Zotenko, E., Bert, S.A., Giles, K.A., Bauer, D.C.*, et al.* (2016). Three-dimensional disorganization of the cancer genome occurs coincident with long-range genetic and epigenetic alterations. Genome Res *26*, 719-731.

Taberlay, P.C., Statham, A.L., Kelly, T.K., Clark, S.J., and Jones, P.A. (2014). Reconfiguration of nucleosome-depleted regions at distal regulatory elements accompanies DNA methylation of enhancers and insulators in cancer. Genome Res *24*, 1421-1432.

Valdes-Mora, F., Gould, C.M., Colino-Sanguino, Y., Qu, W., Song, J.Z., Taylor, K.M., Buske, F.A., Statham, A.L., Nair, S.S., Armstrong, N.J.*, et al.* (2017). Acetylated histone variant H2A.Z is involved in the activation of neo-enhancers in prostate cancer. Nat Commun *8*, 1346.